

DESKTOP MICROFACTORY

by

Zhenishbek Zhakypov

Submitted to the Graduate School of Engineering and Natural Sciences
in partial fulfillment of
the requirements for the degree of
Master of Science

Sabanci University

July, 2013

DESKTOP MICROFACTORY

APPROVED BY:

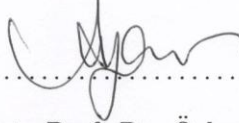
Prof. Dr. Asif Sabanovic, (Thesis Supervisor)

.....


Assoc. Prof. Dr. Ali Koşar

.....

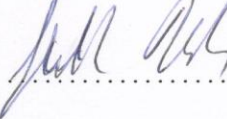

Assoc. Prof. Dr. Ayhan Bozkurt

.....


Asst. Prof. Dr. Özkan Bebek

.....


Asst. Prof. Dr. Ahmet Fatih Tabak

.....


DATE OF APPROVAL: 23. 07. 2013

© Zhenishbek Zhakypov 2013

All Rights Reserved

Abstract

Micro technology is continuously progressing towards smaller, smarter and reliable forms. Consequently, demand for such miniature and complex systems is arising rapidly in various fields such as industry, medicine, aerospace and automotive. Such fast development of micro technology is achieved thanks to improvements in micro-manufacturing tools and techniques. Miniaturization of the machinery and manufacturing equipment is emerging to be an attractive idea that would eventually solve many of the issues existing in conventional micro-manufacturing.

This work presents a modular and reconfigurable desktop microfactory for high precision assembly and machining of micro mechanical parts as proof of concept inspired by the downsizing trend of the production tools. The system is constructed based on primary functional and performance requirements such as miniature size, operation with sub-millimeter precision, modular and reconfigurable structure, parallel processing capability, ease of transportation and integration. Proposed miniature factory consists of downsized functional modules such as two parallel kinematic robots for manipulation and assembly, galvanometric laser beam scanning system for micromachining, high precision piezoelectric positioning stage, camera system for detection and inspection, and a rotational conveyor system. Each of the listed modules is designed and tested for fine precision tasks separately and results are presented. Design comprises development of mechanics, electronics and controller for the modules individually. Once stand-alone operation of each unit is achieved further assembly to a single microfactory system is considered. The overall mechanical structure of the proposed microfactory facilitates parallel processing, flexible rearrangement of the layout, and ease of assembling and disassembling capabilities. These important steps are taken to investigate possibilities of a microfactory concept for production

of microsystems in near future.

Keywords: Microfactory, micro-manufacturing, laser micromachining, micro-assembly, high precision positioning, autofocusing, galvanometric mirror scanner, parallel kinematic robot, walking piezoelectric motor, modularity, reconfigurability.

Özet

Mikro teknoloji devamlı olarak daha küçük, daha akıllı ve daha güvenilir biçimlere doğru mesafe kaydetmektedir. Bunun sonucu olarak bu gibi minyatür ve kompleks sistemlere karşı olan talep; endüstri, tıp, hava-uzay ve otomotiv gibi alanlarda hızla yükselmektedir. Mikro teknoloji alanındaki bu hızlı gelişim ise; mikro imalat aletleri ve tekniklerindeki ilerlemeler sayesinde. Makine ve imalat ekipmanlarının minyatürleştirilmesi ilgi çekici bir fikir olarak ortaya çıkmakla beraber minyatürleşme, er ya da geç geleneksel mikro imalat süresince karşılaşılan problemlerin birçoğunun çözümünü sağlayacaktır.

Bu çalışma mikro mekanik parçaların yüksek hassasiyetli imalatı ve mikro mekanik parçaların işlenebilmesi için oluşturulan modüler ve yeniden yapılandırılabilen masaüstü fabrikayı sunmaktadır. Mikrofabrika; kavram olarak kanıtlanmış ve üretim aletlerinin boyut olarak küçülme eğiliminden esinlenerek ortaya çıkarılmıştır. Sistem temel fonksiyon ve performans gereksinimleri göz önüne alınarak oluşturulmuştur. Bu gereksinimler; minyatür boyut, milimetre altı hassasiyet, modüler ve yeniden yapılandırılabilen yapı, paralel işleme kabiliyeti, taşınabilme ve entegre edilebilme kolaylığıdır. Önerilen mikrofabrika; manipülasyon ve montaj işlemleri için kullanılan paralel kinematiğe sahip iki adet robot, mikro işleme için kullanılan galvonometrik lazer ışın tarayıcı sis-

temi, yüksek hassasiyetli piezo-elektrik konumlama platformu, belirleme ve denetleme işlemleri için kamera sistemi ve dönel taşıyıcı sisteminden oluşmaktadır. Bahsi geçen her bir modül ayrı ayrı olarak, düşük hassasiyet gerektiren görevlerde test edilerek, test sonuçları sunulmuştur. Tasarım; mekanik, elektronik, denetleme modüllerinin ayrı ayrı olacak şekilde geliştirilmesini kapsamaktadır. Her bir modülün bağımsız olarak işlevsel hale getirilmesinden sonraki hedef bu modüllerin mikro fabrikaya monte edilmesidir. Sistemin genel mekanik yapısı; paralel işleyişi kolaylaştırmakta, esnek yeniden ayarlanabilen bir yerleşime olanak sağlamak ve kolay montaj ve demontaj özelliklerini mümkün kılmaktadır. Bu önemli adımlar ise; mikrofabrikaların; yakın gelecekte mikro sistemler üretebilme olanaklarının araştırılması doğrultusunda atılmaktadır.

Anahtar kelimeler: Mikrofabrika, mikro imalat, lazer mikro işleme, mikro montaj, yüksek hassasiyetli konumlama, otomatik odaklama, yürüyen piezo-elektrik eyleyici, galvonometrik ayna tarayıcısı, paralel kinematik robot, modülerite, tekrar konfigüre edilebilme.

Acknowledgements

I would like to express deep gratitude to my supervisor Prof. Dr. Asif Sabanovic for academic mentorship, moral support and valuable advices throughout my academic life as a Master student. I highly appreciate my thesis jury members Assoc. Prof. Dr. Ali Koşar, Assoc. Prof. Dr. Ayhan Bozkurt, Asst. Prof. Dr. Özkan Bebek and Asst. Prof. Dr. Ahmet Fatih Tabak for showing interest in my work.

I also would like to convey my special thanks to Edin Golubovic for being not just a good colleague of mine but a helpful teacher in early stages of my research life. I thank my laboratory colleagues Tarık Edip Kurt, Ahmet Özcan Nergiz, Tarik Uzunovic and Eray Baran for contributions and valuable discussions on various topics and particularly on this thesis.

Special thanks to my close friends Murodzhon Akhmedov and Tarık Edip Kurt for personal support and bringing joy to my life.

My deepest gratitude to my parents for letting me walk on the road of wisdom and knowledge.

I would finally like to acknowledge Yousef Jameel Scholarship Fund for partial financial support.

TABLE OF CONTENTS

Abstract	iv
Özet	v
Acknowledgements	vii
List of Tables	xi
List of Figures	xii
1 INTRODUCTION	1
1.1 Motivation	1
1.2 Objectives	2
1.3 Thesis organization	4
2 STATE OF ART	5
2.1 Micro-manufacturing and microfactory	5
3 PROBLEM FORMULATION	11
3.1 Design requirements for micromanufacturing	11
3.1.1 Small size	12
3.1.2 High precision	12
3.1.3 Modularity	13
3.1.4 Reconfigurability	14
3.1.5 Energy efficiency	14
3.1.6 Productivity	15
3.1.7 Portability	15
3.2 Functional modules	15

4	DESIGN AND IMPLEMENTATION	17
4.1	Microfactory mechanical structure and functional modules	17
4.2	Rotational Intermodular Transportation Mechanism	22
4.2.1	Positioning Issues	23
4.2.2	Positioning experiments and results	24
4.3	Parallel Kinematic Robots	26
4.3.1	Delta robot description	26
4.3.2	Experiments and Results	27
4.4	Autofocusing Inspection System	30
4.4.1	Camera system description	30
4.4.2	Experimental Results	31
4.5	Galvanometric Laser Beam Steering System	33
4.5.1	System Overview	34
4.5.2	Kinematics of the system	35
4.5.3	Reference image generation	39
4.5.4	Model tuning and verification	40
4.5.5	Controller approach	41
4.5.6	Experimental results	42
4.6	High precision positioning stage	49
4.6.1	Walking piezoelectric motor	50
4.6.2	Operation in discontinuous mode	53
4.6.2.1	Experimental verification of step size to applied voltage dependence	56
4.6.2.2	Adaptive Controller Design	58

4.6.2.3	Piezo walker driving electronics design	61
4.6.2.4	Experimental results	65
4.6.3	Operation in continuous mode	68
4.6.3.1	Dynamical model of the legs	68
4.6.3.2	Static model and identification	71
4.6.3.3	Dynamical model parameters identification	73
4.6.3.4	Controller scheme	75
4.6.3.5	Experimental results	77
4.6.4	High precision positioning stage design	79
4.7	Software Design	81
4.7.1	Software Organization	81
4.7.2	Human Machine Interface	87
4.7.2.1	GUI	87
4.7.2.2	Software/Hardware interface	89
5	CONCLUSION AND FUTURE WORK	91
A	APPENDIX A	93

List of Figures

2.1	First prototype of desktop microfactory, MMC and MEL, Japan . . .	5
2.2	Miniature micro lathe for microfactory	6
2.3	Desktop microfactory prototype [4]	7
2.4	Miniature CNC machine [5]	7
2.5	Manipulator types	8
2.6	Reconfigurable micro milling - micro turning machine prototype [27] .	9
2.7	Reconfigurable microfactory developed by Tampere University of Technology [14]	10
3.1	Modularity and reconfigurability in manufacturing	14
3.2	Some functional modules and their application	16
4.1	CAD design of a microfactory	17
4.2	Microfactory top view	18
4.3	Assembled microfactory system	20
4.4	Closer view to microfactory system	21
4.5	Adjustable mechanical connectors	21
4.6	Rotational intermodular transportation mechanism structure	22
4.7	Possible examples of sample plates	23
4.8	Geometrical relation of rotational angle to translational positions . .	23
4.9	10° reference stair case response	25
4.10	Parallel Kinematic Delta Robot	26

4.11	Delta robot experimental setup	27
4.12	(a) 2 mm circle reference ($f = 2\text{Hz}$) (b) Corresponding motor angle ref. vs. actual position	28
4.13	(a) 2 mm circle reference ($f = 4\text{Hz}$) (b) Corresponding motor angle ref. vs. actual position	28
4.14	1mm radius $f=4\text{ Hz}$ circle reference (a) ref. vs. sensor (b) ref. vs. encoder	29
4.15	0.1mm radius $f=1\text{ Hz}$ circle reference (a) ref. vs. sensor (b) ref. vs. encoder	29
4.16	Autofocusing camera system	30
4.17	Autofocusing experimental results	32
4.18	Galvo laser beam scanning system	35
4.19	Laser beam reflection geometry by means of galvo mirrors	36
4.20	System behavior in x coordinate	38
4.21	System behavior in y coordinate	38
4.22	Overall system block diagram	40
4.23	100 μm circle PSD to OPS measurement plot	41
4.24	100 μm circle PSD to OPS measurement error plot	41
4.25	Galvo experimental setup	43
4.26	250 μm radius circle reference tracking response	44
4.27	250 μm radius circle reference tracking error	44
4.28	50 μm radius circle reference tracking response	45
4.29	50 μm radius circle reference tracking error	45

4.30	1 mm size rectangular "G" letter reference tracking response	46
4.31	1 mm size rectangular "G" letter reference tracking error	46
4.32	100 μm size rectangular "G" letter reference tracking response	47
4.33	100 μm size rectangular "G" letter reference tracking error	47
4.34	50 μm and 150 μm radius marked circles	48
4.35	400 μm marked rectangular letter "G"	48
4.36	PiezoLEGS motor structure	51
4.37	Principles of motor operation in stepping and bending modes	52
4.38	Legs tip trajectory with varied phases (black) and a half amplitude (red)	55
4.39	Amplitude to step dependence plot	57
4.40	Phase shift to step dependence plot	57
4.41	Frequency to velocity dependence plot	58
4.42	Frequency to absolute error plot	60
4.43	Amplitude to absolute error plot	60
4.44	Adaptive controller scheme	61
4.45	Commercial driver PDA 3.1	62
4.46	Analog voltage amplifier board	63
4.47	Half bridge switching converter board	63
4.48	Half bridge converter schematic	65
4.49	Single dimensional piezo motion stage	66
4.50	100 μm step reference response	66

4.51	100 μ m step reference response, zoomed	67
4.52	500 μ m stair case reference response	67
4.53	500 μ m stair case reference response, zoomed	68
4.54	Legs and rod MSD model in y coordinate	69
4.55	Legs and rod MSD model in x coordinate	71
4.56	Rod displacement in y direction vs. sum of phase voltages	73
4.57	Rod displacement in x direction vs. difference of phase voltages	73
4.58	Actual and estimated system step response plots	75
4.59	50 nm stair case response	77
4.60	50 nm stair case error	77
4.61	10 nm stair case response	78
4.62	10 nm stair case error	78
4.63	100 nm p-p sinusoidal reference tracking response	78
4.64	Two dimensional high precision positioning stage CAD drawing	79
4.65	Manufactured and assembled high precision positioning stage	80
4.66	Piezo calliper motor scheme	81
4.67	Possible system organization	83
4.68	Possible process flow	83
4.69	Sample plate organization	84
4.70	Microfactory GUI, Laser control panel	88
4.71	Microfactory GUI, Vision control panel	88

4.72 Software to hardware interface structure	89
4.73 Main and delta robot board schematics	90

1 INTRODUCTION

1.1 Motivation

Today's technology is continuously transforming from greater size to more compact, denser and smarter forms. It enables ease of integration of the miniature devices in various fields such as medicine, aerospace and automotive industry where small size, high performance and precision are of great interest. Demand for such devices is rapidly increasing, creating manufacturing issues in quick and reliable product supply. So, with the miniaturization of products a consequent demand for relevant fine precision manufacturing machines arises. Nowadays, relatively large manufacturing machines are employed to produce technology in micro scales such as semiconductor chips, MEMS, micro actuators and sensors. Main disadvantages of such production tools are their bulky size, high power consumption and excessive material usage that creates problems in economic, transportation, maintenance and environmental aspects.

Active research has been conducted for last two decades in order to improve existing manufacturing techniques and solve these issues. Researchers come up with an innovative idea of micro product processing so called "Microfactory". Very first notion of the concept was proposed by the Micro Machine Center and Mechanical Engineering Laboratory (MEL) in Tsukuba as a part of the Japanese national project "Micro Machine" in 1990 [1]. Simple idea behind microfactory is to use accordingly small machines for manufacturing of small parts or systems. With the development of tiny and precise actuators, and also accurate measurement devices, challenging opportunities for downsizing of the machinery are appeared and by that possibility

to develop miniature manufacturing mills is created. Important key advantages of such miniature factory lay in environmental, technical and human related factors [2]. Microfactory due to its small mechanical structure could significantly reduce material usage, decrease vibrations, noise and pollution. It can be economically effective because of reduction in running costs such as power consumption, air conditioning, clean room operation, illumination and portability. Low inertias enable higher speed and precise operation. Small size, low weight and modular design allows ease of reconfigurability of the machines. Custom configuration can be easily achieved by rearrangement of the processing tools or just replace them by different type which is almost unfeasible with big and heavy machines. Moreover, flexible and compact design will allow to easily operate the machines by technical staff. Also ease of transportation opens a door to possible operation of the microfactory not only in industrial facilities but run them to produce custom items at offices, home and educational organizations.

Microfactory concept has a wide range of innovational advantages and not only limited to the mentioned ones. Though it is an attractive idea, still much investigation of the concept is required. Since cost of high precision micro equipment still remains extremely expensive more cost effective solutions should be developed without deteriorating system performance, hence cheaper measurement devices and actuators for micro/nano precision applications are of great concern.

1.2 Objectives

Aim of this thesis work is to design and implement a desktop microfactory as a proof of concept for micromanufacturing. Steps are taken towards the investigation of a microfactory design and its possible application for production of sub millimetre size micro-electromechanical systems in near future. Efforts are dedicated to the solution

or partial improvement of some crucial issues existing in conventional manufacturing systems such as size, precision, speed, productivity, modularity, reconfigurability, material usage and transportation. For this purpose a miniature microfactory is built with parallel processing, modular, reconfigurable and user friendly functional characteristics. The proposed design has a compact size in order to be used for desktop applications. It's low weight enables ease of transportation and installation. Parallel processing is permitted thanks to rotational structure of a conveyor mechanism for parts delivery to the functional modules placed in parallel manner. Compared to serial approach, parallel operation of each unit allows fast processing and consequently improves productivity. Modular structure is an important asset of the proposed design. Processing units can be removed, replaced or reconfigured with respect to production goals. Frame structure facilitates flexible adjustment of the modules by means of adjustable mechanical connectors.

Overall system consists of functional modules that accomplish certain high precision tasks. Main functions include microassembly, pick-place, micromachining by means of high power laser, microscopic inspection and precise positioning of micro parts. Functional units such as two parallel kinematic robots, high power laser with galvo mirror scanning system, autofocusing vision system, high precision positioning stage and intermodular transportation mechanism are employed to achieve these goals. Each unit is designed separately in the beginning and tested for some performance criteria. Mechanics, electronics and controllers are fully or partially designed for each module separately to allow operation in both stand-alone and cooperative configurations. Organization of the modules to a single desktop microfactory system creates possibility to replace conventional micro technology production factories with miniature, more reliable and flexible micromanufacturing plants in the future.

On the basis of existing issues in manufacturing of microsystems a research in micro-

factory is launched to overcome problems mentioned above and to prove the concept of an innovative micromanufacturing system. Author contributed to the research in various aspects such as overall mechanical design of the microfactory system, design and precise control of three particular functional modules such as galvanometric laser beam steering system for micromachining, high precision piezoelectric positioning stage and rotational intermodular transportation system for micro-part delivery. Rest of the modules such as parallel kinematic robot and autofocusing vision system are developed within the context of other works also referenced in the upcoming sections.

1.3 Thesis organization

This thesis is organized as follows; in Chapter 2, the state of art in micromanufacturing and microfactory is provided discussing past and current progress in this field. Also, important developments regarding micromachining, microassembly and other micro-processing fields are presented in details. In Chapter 3, the problem formulation of a microfactory, micromanufacturing system design requirements with necessities and challenges for the development of the microfactory concept are described. The design and implementation of a modular desktop microfactory and processing modules under consideration in this work is described in Chapter 4, also presenting experimental results. Thesis is concluded in Chapter 5 with discussions on achieved goals and possible future work.

2 STATE OF ART

2.1 Micro-manufacturing and microfactory

The very first microfactory prototype was introduced by Japanese researchers in early 1990s with the introduction of a desktop machining microfactory (see Fig.2.1) by the Micro Machine Center (MMC) and the Mechanical Engineering Laboratory (MEL) of the Agency of Industrial Science and Technology (AIST), Japan [1]. This research is addressed to miniaturization of manufacturing machines for production of mechanical parts of sub-millimeter size.

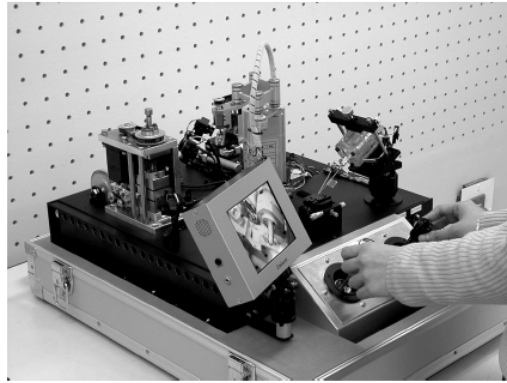


Figure 2.1: First prototype of desktop microfactory, MMC and MEL, Japan

The miniature factory is a chain of machining and assembly units capable of manufacturing micro bearings with dimension of 0.9 mm. The functional units involved in production are: a micro lathe, micro drill, micro press, transfer robot and a manipulation robot. The dimensions of the whole system are $625 \times 490 \times 380 \text{ mm}^3$ with a weight of 34 kg that enables ease of transportation. Micro lathe is the smallest element within the system which can fit in human arm as depicted in Fig.2.2 and

weights only 100 g. Thin needle of 50 μm diameter and 600 μm long was successfully machined out of brass with this device.

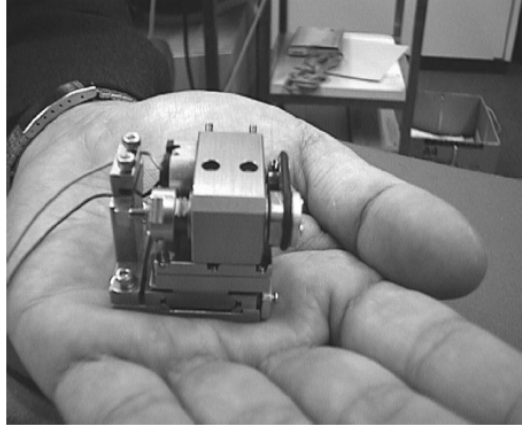


Figure 2.2: Miniature micro lathe for microfactory

Steps towards miniaturization and microfactory concept presented advantages over conventional production equipment in various aspects such as energy and material savings, improvements in accuracy, speed of operation and ease of transportation. For more than 20 years researchers are investigating possibilities of the concept and its future trends in quick and flexible manufacturing of microsystems for industrial, aerospace, automotive, medical and many other applications. Several microfactory concepts and miniaturized production systems are presented in literature till now [1-5]. One possible application targets machining and assembling of tiny gears for mechanical watches [4] with desktop microfactory concept.

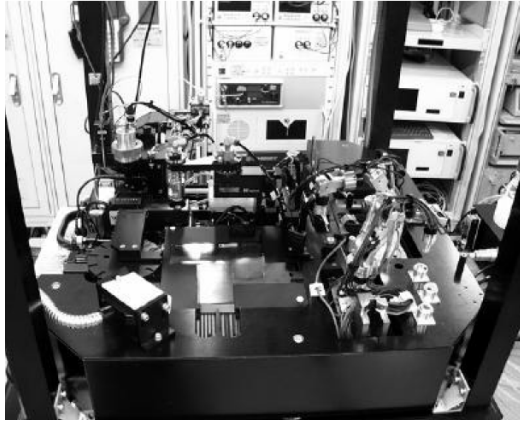


Figure 2.3: Desktop microfactory prototype [4]

With the tendency to miniaturize tools, a shift from conventional huge CNC machines to mini CNC devices for machining tiny mechanical parts become possible [6,7].

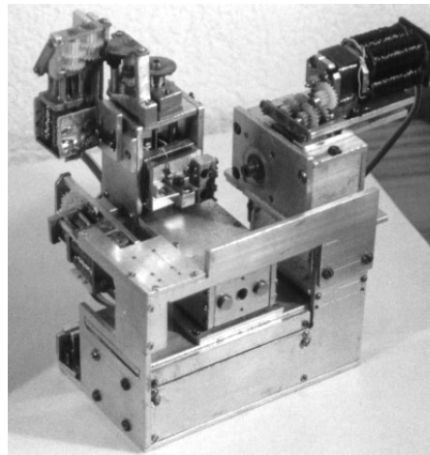


Figure 2.4: Miniature CNC machine [5]

Miniaturization opened a door to wide range of research topics in micromanufacturing such as micromachining, microassembly, micromanipulation, microrobotics and etc. Most of the systems are considered for assembly of very small parts or products by employment of micromanipulators and gripping mechanisms [8-12]. As

in conventional assembly lines designers make use of miniature multiple degree of freedom serial and parallel manipulators as depicted in Fig.2.5.

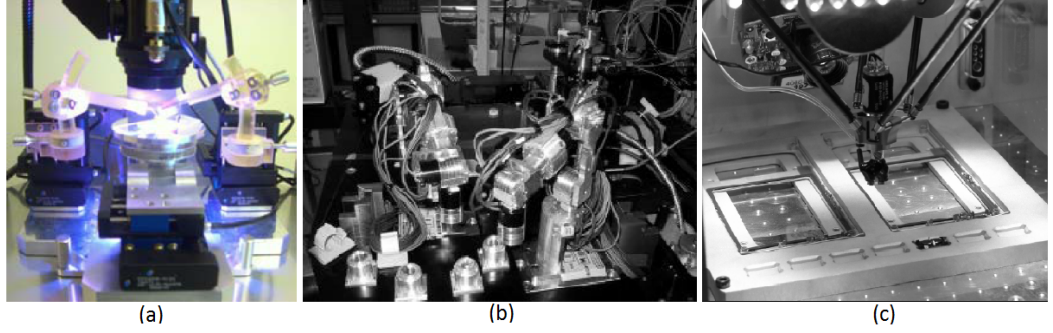


Figure 2.5: Manipulator types

Assembly is generally performed by means of multiple manipulators as shown in Fig. 2.5 (a) [13], single serial robotic arms (b) [4] or parallel kinematic robots (c) [14]. Microrobots [15,16] and mobile microrobots [17] are also common for performing assembly tasks. They are used in single or cooperative manner depending on complexity of the duty. Main advantage of mobile microrobots is their mobility and flexibility to work within structures where fixed machines unable to reach. Occasionally, microsystems assembly may require clean and contamination free environment. For this purpose more economic microfactory with clean room properties is possible to design due to miniaturization of machinery [18].

Micromachining is also crucial and of great demand within microfactory context because there may be a necessity for mechanical parts with desired structure and dimensions. One crucial advantage of machining tools in microfactory can be a quick prototyping of custom medical devices, implants and mechanical parts for specific purposes at hospitals, home and offices. Custom 2D and 3D mechanical structures can be developed with employment of several types of machining equipment along with several techniques. Main approaches comprise micro-mechanical cutting with direct mechanical material removal [19,20], electrical-discharge machining (EDM)

by thermal effect [21,22], micro-electrochemical machining (ECM) by chemical process [23], laser machining with minimised focus resolution [24,25]. Miniature micro milling machines [26] and micro turning machines [27] are also employed as micro-factory modules. Besides the presented solutions with material removal there is also a potential application of micro-forming techniques [28] to form a desired mechanical shapes in 3D.

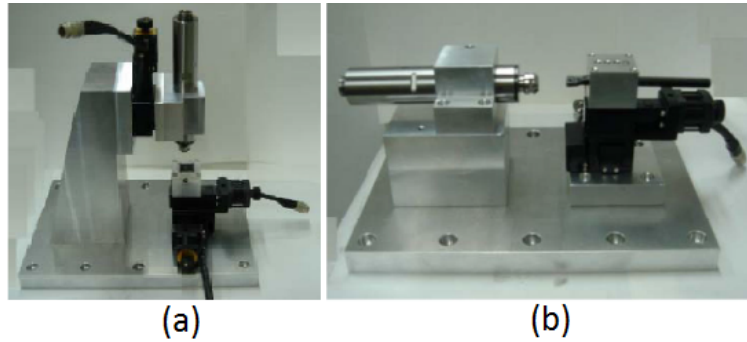


Figure 2.6: Reconfigurable micro milling - micro turning machine prototype [27]

Along side with the development of the necessary technology for micro manufacturing, new research directions are also emerged towards modularity and reconfigurability concept in microfactory systems. Module is a machine or a group of machines that may operate in stand-alone or cooperative way with other units. This operation can be classified as task or process oriented depending on factory layout [29]. Thus few modules create a set of processing phases and can be easily reconfigured to different layout depending on production goals. Hence it adds another flexibility to manufacturing of customized products [14,30,31].

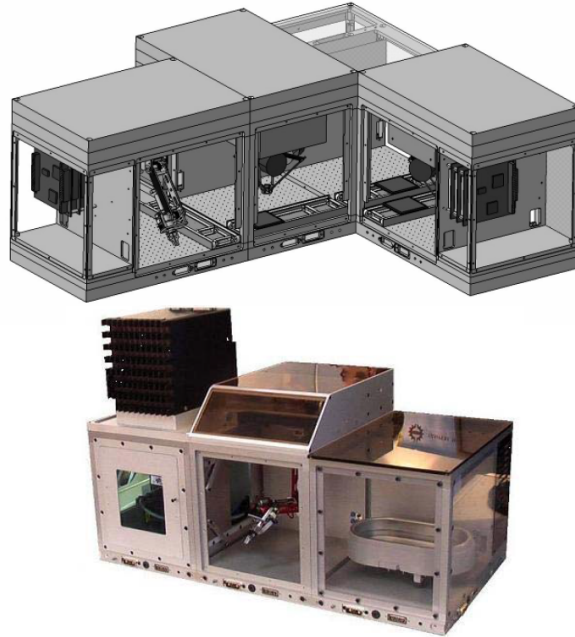


Figure 2.7: Reconfigurable microfactory developed by Tampere University of Technology [14]

3 PROBLEM FORMULATION

3.1 Design requirements for micromanufacturing

Processing in micro scales should be performed precisely to achieve accurate results because in this range every micron does matter. Therefore production machines to be used in manufacturing of microsystems should meet some important performance criteria. While constructing a miniature factory system the main performance requirements for an accurate design are:

- Small size: smaller size machines result in more material and workspace savings;
- High precision: micro parts are required to be manufactured accurately therefore production machines need accordingly maintain high precision operational capabilities;
- Modularity: each processing device or module need to be self-sufficient with it's own software and hardware for stand alone operation;
- Ease of re-configurability: system should allow reconfigurability of the modules depending on production goals. It adds more flexibility to manufacturing customized products by interchanging or replacing the processing units;
- Energy efficiency: low power consumption is important for cost effective production. Hence system should consist of low power devices such as low torque actuators and measurement sensors;
- Productivity: it is crucial for fast and efficient product development. Enabling fast and parallel processing one can significantly improve productivity;

- Portability: compact size and low weight systems will allow ease of transportation of the system.

By satisfying the listed requirements above one can guarantee precise and efficient operation of the system consequently a high quality of manufactured goods. Microfactory can be one of the most potential solutions that fits to these criteria from many aspects. The advantages and design necessities of such approach are discussed from now on.

3.1.1 Small size

Miniaturization is the main goal of a microfactory system design. It characterizes several benefits in material and performance aspects. Material usage, workspace coverage and complexity of the mechanical structure is highly related to the size of the machines. Downsizing is favorable for material savings because smaller volumes require less material usage. It also requires less workspace to cover thus smaller workshops or facilities can be utilized with less rental costs. Microfactory with desktop operation concept can be integrated to various environments such as workshop, office, hospital, home or garage. Also more tiny machining units can be employed instead of few big machinery to increase production. Ease of maintenance is another advantage of miniature structure.

3.1.2 High precision

In order to come up with miniature, accurate and complex products microfactory needs to comprise high precision processing capabilities. Satisfactory results can be achieved by incorporating precise actuators and fine measurement devices are no more new. Currently, tiny actuators with few micro meters positioning accuracy and digital encoders with few nanometers measurement precision are available in the market.

Besides that mechanical design of machining, assembly and positioning devices may have a great impact on working performance. Therefore an accurate, backlash-free and fine mechanical design should be considered for high precision operation. Finally, appropriate control techniques should be employed for compensation of system uncertainties, guarantee the desired, precise and robust system response for input references.

3.1.3 Modularity

Modularity can be easily attained by miniaturization of micromanufacturing equipment. Modular design adds flexibility to overall system assembly and reconfigurability. For this purpose functional goals of a miniature factory should be set by the designer at the beginning and processing modules are designed accordingly. It is a matter of simplicity to construct each module separately and test for specific performance criteria before integrating into the microfactory system for collaborative tasks. Modules are required to be self-sufficient with their individual control software and hardware for independent operation. For instance, a machine should have its own controller, interface electronics and necessary mechanical components to be easily incorporated into the system for cooperative tasks with other modules or operate independently in stand-alone configuration. Once this demand is satisfied, system is named to be modular.

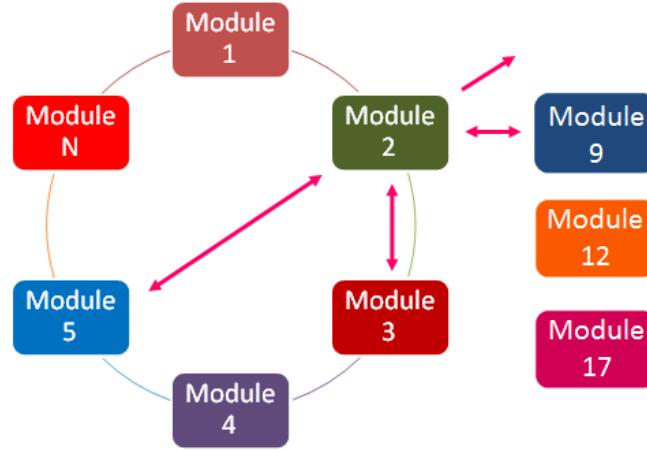


Figure 3.1: Modularity and reconfigurability in manufacturing

3.1.4 Reconfigurability

Small size, light weight and modularity bring another advantage to the system such as reconfigurability. System is said to be reconfigurable if layout of the modules can be modified according to production goals. It is almost unfeasible to reconfigure processing tools in conventional factories because of heavy and bulky nature of the machines. Hence it is beneficial to acquire dynamic configuration of the machinery with microfactory concept. Any module can be removed or replaced by another type so flexibility can be attained with this approach. System can be set to task or process oriented configurations. In task oriented approach some modules can be configured according to smaller tasks where in process oriented method system can be adjusted according to several tasks or processes.

3.1.5 Energy efficiency

It is favorable to build reliable and energy efficient technology. Generally, in conventional factories a lot of energy is consumed by huge machines moved by high torque electrical drives, illumination lamps, air-conditioning, clean room facilities and etc.

For lighter and low inertia designs lower torque actuators can be employed to drive particular mechanisms. Also small workspace can significantly improve energy efficiency because smaller and lower power equipment can be employed.

3.1.6 Productivity

Lower inertia allows to achieve higher speeds of operation. Faster the processing the more products can be developed in particular span of time. So, high velocity actuators should be considered for this purpose. In addition to quick response characteristics, parallel processing can surely increase productivity of the microfactory. Compared to serial production, parallel operation of each module would result in immediate product processing without awaiting in the line.

3.1.7 Portability

Miniature, light and self-sufficient factory can be simply transferred from one place or environment to another. Desktop microfactory concept enables wide range of environments where it can be installed such as workshops, home, offices, hospitals or schools. It creates opportunities for fast prototyping and manufacturing of custom components by every user with no prior deep knowledge of manufacturing. Moreover, portable design is suitable for mobile productions in the vehicle while transporting the system. Such method merges production and transportation time, and speeds up the product delivery.

3.2 Functional modules

Micro-manufacturing systems generally consist of several machines that have specific functional and operational purposes. It may compose of several manipulation robots, machining tools, inspection cameras and conveyor mechanisms for micro specimen

delivery. These devices are generalized as modules or units. Modules can be classified according to functional characteristics as follows:

- Manipulation: assembly, pick-place, gripping of the micro parts, microinjection of biological cells;
- Machining: mechanical, laser, EDM, electrochemical material removal;
- Inspection: microscopes, vision sensors, CCD cameras for detection and image processing;
- Transportation: linear and rotational stages, belts, pressure, pumps for micro-particle sample delivery.

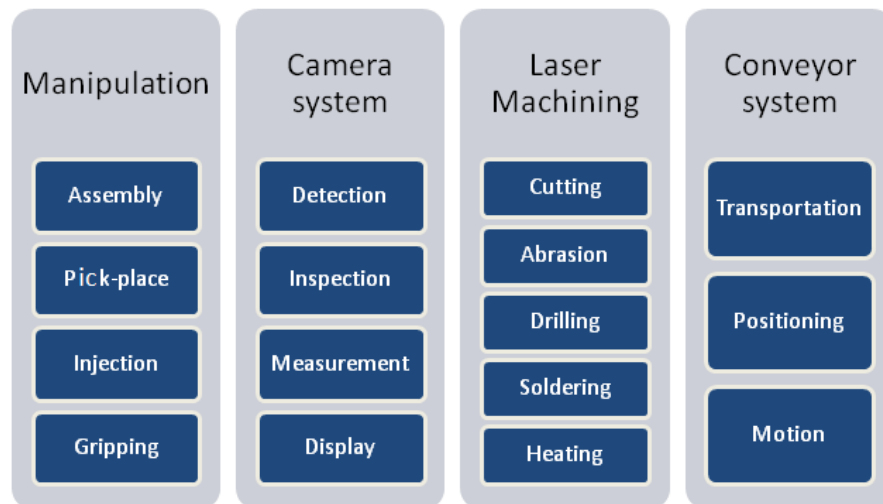


Figure 3.2: Some functional modules and their application

4 DESIGN AND IMPLEMENTATION

4.1 Microfactory mechanical structure and functional modules

Mechanical design CAD drawing of the proposed microfactory system are depicted in Fig. 4.1 and view from top in Fig. 4.2, respectively.

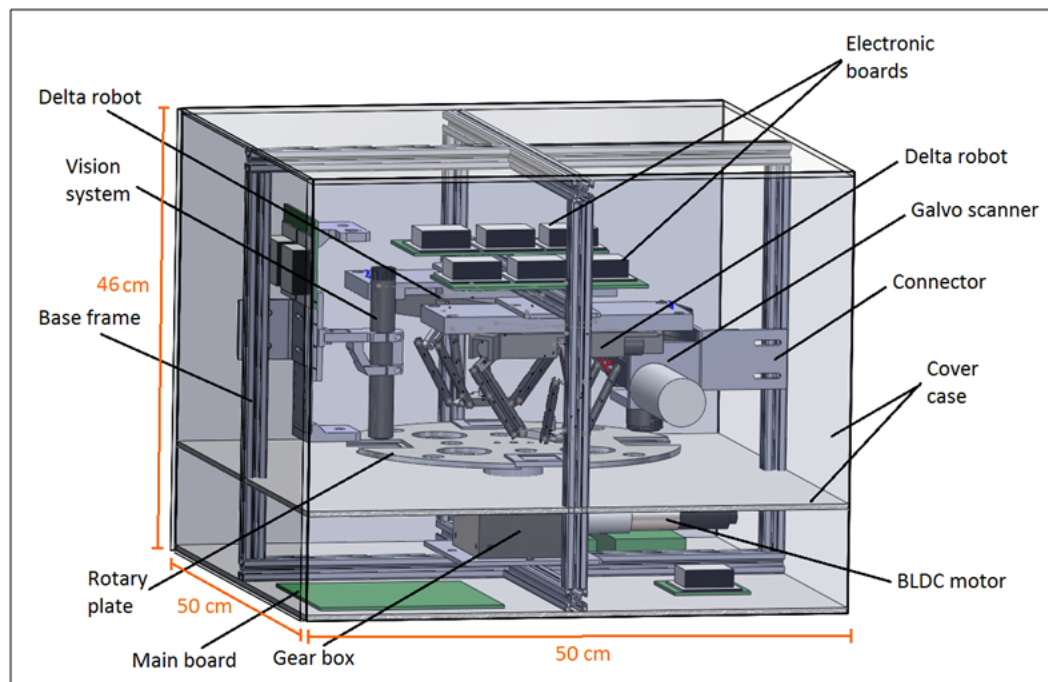


Figure 4.1: CAD design of a microfactory

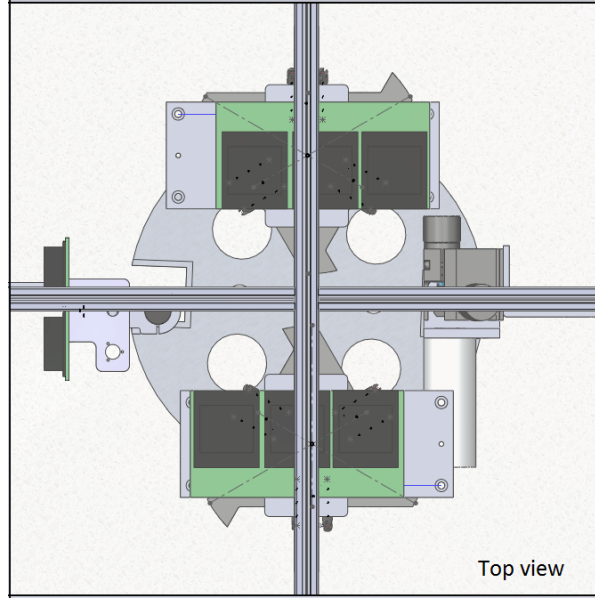


Figure 4.2: Microfactory top view

The structure is compact in size and has dimensions only of $50cm \times 50cm \times 46cm$ which makes it suitable for desktop applications with vibration free operation. Overall design including the processing modules is made up of low weight metals such as aluminum accordingly structure is light with a mass of approximately 15 kg that enables ease of transportation and integration to other environments. Flexible mechanical structure, custom readjustment of the overall design and cheap installation costs are the main advantages of the proposed system over the ones presented in the literature. It is mainly due to the approach used similar to conventional industrial automation setups with employment of small sigma profiles. These profiles are considered for supporting base frames. Standard aluminum sigma profiles are available in the market with different size options for low cost. Another advantage is their low weight but stiff structural nature. It's structure adds flexibility to assembly and disassembly of mechanisms or tools by means of screws. It can be easily adjusted to a desired length by simply cutting of the material. Therefore overall design of the microfactory can be modified quickly and cost effectively to a desired structure.

Sigma profiles are connected to each other at the ends resulting in a prismatic base frame of the microfactory. Four modules are assumed to be mounted to four columns at the corners of the frame in order to allow parallel processing capability of the current design. Thus all four modules are able to operate at the same instant of time. Such configuration clearly accelerates production and increases the productivity of the factory. Once each unit accomplishes its own task, next task is carried out after the rotation of the conveyor plate and delivery of a new sample to the modules. Rotational conveyor mechanism consists of a gear box with high gear ratio and a circular plate mounted on it. It performs accurate and backlash-free positioning of specimen to a processing module in question. Ergonomic metallic connectors are considered module attachment to sigma frames as depicted in Fig. 4.5. Such design is suitable for attaching the machines and adjusting them to desired position in all x-y-z axis for better operational performance.

The proposed design consists of five main functional modules: two parallel delta robots for pick-place, assembly and manipulation, galvanometric mirror laser scanner system for micromachining and marking, auto focusing vision system for detection of micro particles and position feedback, and rotational intermodular transportation mechanism (RITM) for micro part delivery. Modules are designed and tested separately from the point of mechanics, electronics and control at the beginning. Details of each module design are described in the upcoming sections. For the sake of modular design modules are built in self-sufficient manner thus each unit contains its own particular hardware and control software. Electronic boards (see green colored blocks in Fig. 4.1) are developed to maintain connection between modules and the operator computer. It also contains necessary motor drive electronics residing on it. In this manner each module can function independently of each other in stand-alone configuration for single task or employed for collective processes. It adds reconfigurable

characteristics to the system therefore any module can be interchanged or replaced by different type according to production goals.

The manufactured and assembled design of the desktop microfactory with all of the modules mounted is given in Fig. 4.3 and the closer view is provided in Fig. 4.4.

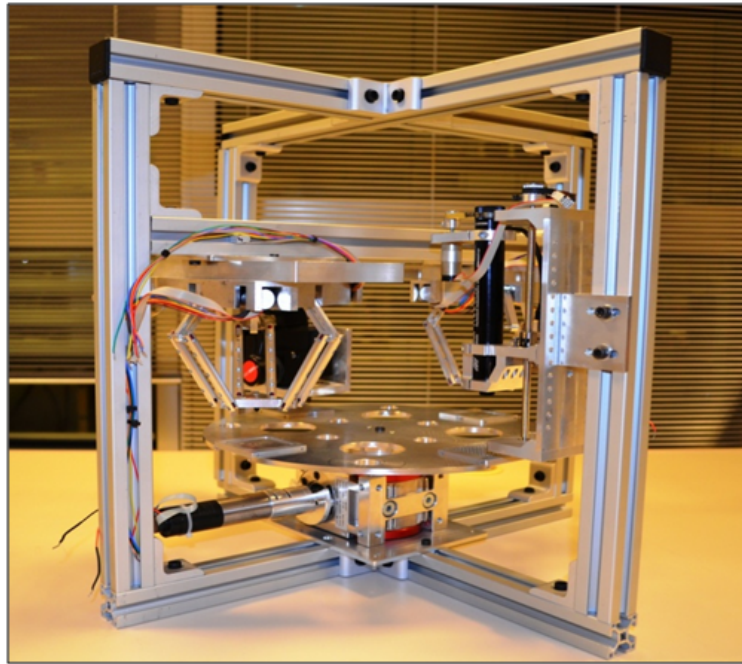


Figure 4.3: Assembled microfactory system

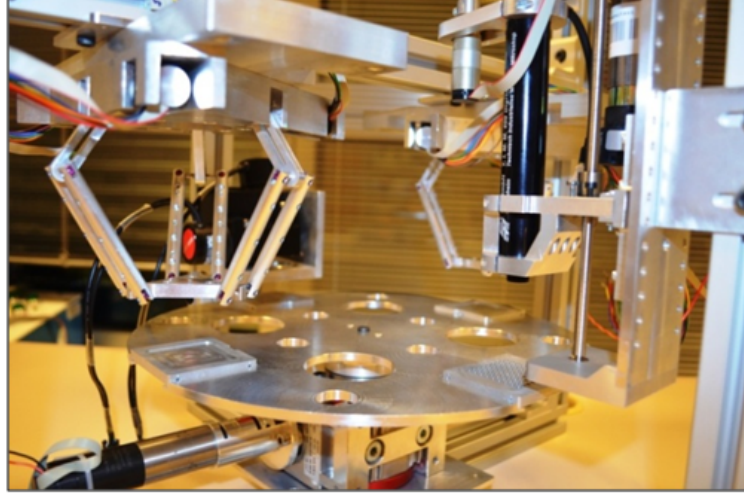


Figure 4.4: Closer view to microfactory system

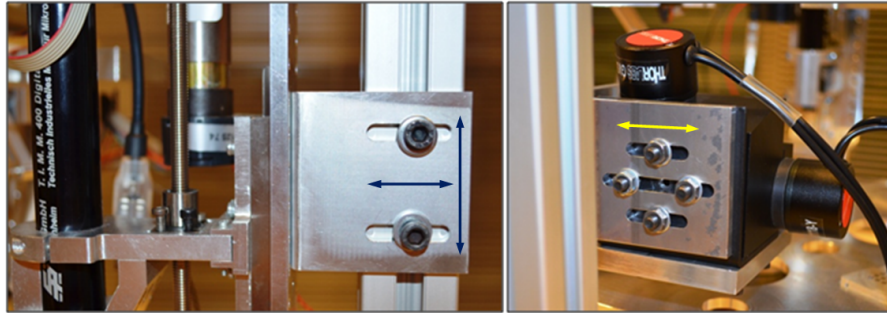


Figure 4.5: Adjustable mechanical connectors

Description of design and improvement steps of each module for high precision applications are provided in further sections. Experimental results are presented in order to assess performance of the units. Within the scope of the thesis development details of only some modules such as rotational intermodular conveyor system, galvo laser beam scanner and high precision positioning stage are presented where author was directly involved in design process. Also brief information and experimental results for parallel kinematic delta robot and autofocus vision system are introduced in order to present full picture of the proposed microfactory concept.

4.2 Rotational Intermodular Transportation Mechanism

Rotational Intermodular Transportation Mechanism (RITM) is depicted in Fig. 4.6. The role of the RITM is to convey samples to be manufactured to a desired processing module. After each unit accomplished its task, the circular plate rotates and carries samples to the next unit in question for further processing. Final product is assumed to be ready after one whole rotational cycle of the plate. Mechanism is driven by a 12 V brushless DC motor coupled to a rectangular gear box with gear ratio of 47:1. Electrical drive is nominally comprises gear head with 43:1 ratio and digital encoder inside for reading angular positions. The mechanism structure enables parallel processing with more precise and backlash-free positioning capabilities that are important assets in micro-positioning compared to conventional conveyor belt mechanisms.

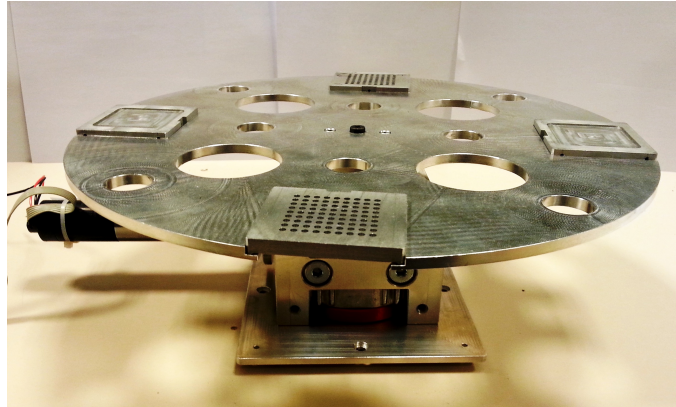


Figure 4.6: Rotational intermodular transportation mechanism structure

Circular plate has a 30cm diameter and 5mm thickness. It contains of four rectangular cell spacings at the edges with 90° angular separations for placing sample plates on which micro parts to be machined can be sited. The main advantage of such approach is that sample plate's internal pattern may vary with the size and

dimensions of micro parts and can be product specific without affecting the whole circular plate structure (refer to Fig. 4.7). They can be easily removed or replaced by different type if necessary. Hence it adds flexibility on machining any micro product without modifying the whole design.

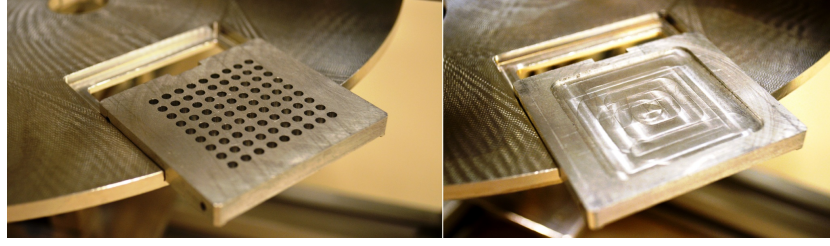


Figure 4.7: Possible examples of sample plates

4.2.1 Positioning Issues

Positioning of the RITM should be performed precisely because any variations or errors in positioning may consequently degrade the operational accuracy of the modules. For this particular design a 90° angle of rotation is expected ideally with the completion of each task. Any small deflection in rotational angle greatly effects translational positioning of a specimen. This phenomena is demonstrated in Fig. 4.8.

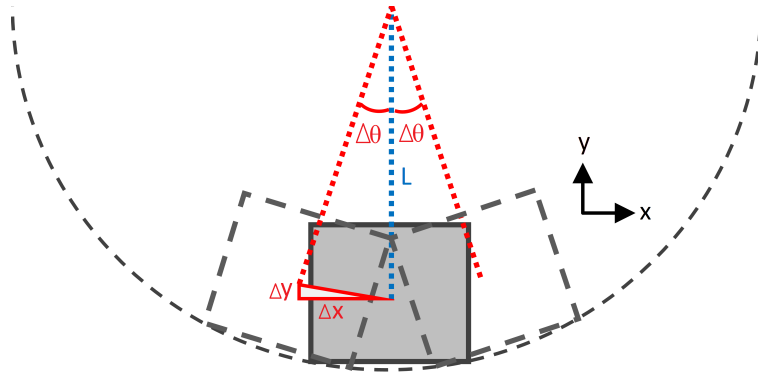


Figure 4.8: Geometrical relation of rotational angle to translational positions

From the figure it can be noticed that any small rotational error $\Delta\theta$ results in

translational errors Δx and Δy that surely effects overall system performance. Thus errors in rotational space should be minimized in order to minimize errors in positioning of the samples. This relation can be expressed by examining geometry of the plate rotation. Let L be the distance between the centers of circular plate and rectangular sample plate. Then a small error in positioning $\Delta\theta$ in one direction can be mapped into errors in Δx and Δy on $x - y$ coordinate plane

$$\Delta x = L \sin \Delta\theta \quad (4.1)$$

$$\Delta y = L(1 - \cos \Delta\theta) \quad (4.2)$$

From the equations it can be clearly inferred that errors in $x - y$ plane greatly depend on both the radius of the circular plate and the error in rotational space. For the rotary plate under consideration in this design L has a value of approximately $125mm$. For instance, if error in positioning of approximately 0.01° mechanical degrees is assumed then deviation of the positions in translation space can be calculated as $\Delta x = 21.8\mu m$ and $\Delta y = 1.9nm$. So by minimizing errors in positioning angles one can minimize positioning error in $x - y$ coordinates.

4.2.2 Positioning experiments and results

The role of RITM is to rotate and accurately deliver the specimen to the workspace of a module in question for further processing operations. Since samples are placed 90° from each other the control of positioning with right angles should be precise. Therefore, for this model a PI controller is used to reach a desired performance in positioning. Experimental results for stair case reference inputs with the controller under consideration is provided in Fig. 4.9).

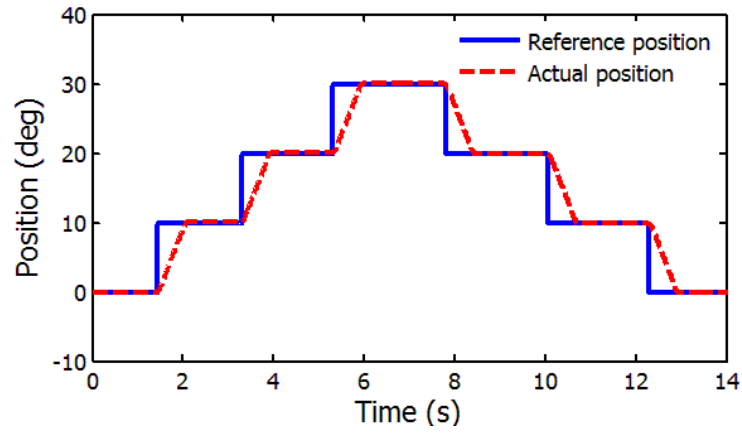


Figure 4.9: 10° reference stair case response

The positioning results with this controller is precise enough to meet the operational needs of the processing modules without degrading precision of the system. The response is relatively slow to reach the desired position due to the double stage of high ratio gear head of a DC motor and the external gear box. However, positioning in few seconds is negligible for such simple delivery tasks.

4.3 Parallel Kinematic Robots

4.3.1 Delta robot description

Manipulation is one of the crucial functions in manufacturing since parts should be moved or manipulated by some exertion of external actions if necessary. Manipulator mechanisms can be used for gripping, pick-place, assembly or injection purposes. Precision and speed of manipulation is an important asset especially in micromanufacturing. For this purpose two parallel kinematic robots are developed to accomplish microassembly and pick-place tasks (refer to Fig. 4.10). Crucial advantage of parallel mechanisms over serial robots is their more precise, faster and stiffer performance characteristic. The main drawback of parallel robots is limited operational space due to complex correlated structure of the mechanisms. However for micro-manipulation applications where small workspace is concerned this shortage can be disregarded.

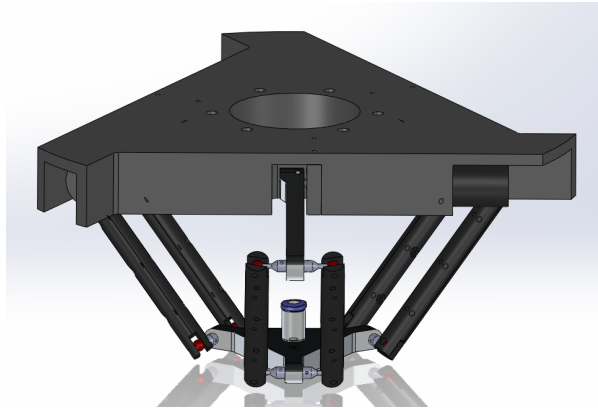


Figure 4.10: Parallel Kinematic Delta Robot

Final prototype of the robot is compact in size with 40 mm^3 operational space volume. It has three metallic arms mounted to backlash-free BLDC motors at the base and connected to triangular frame on the other end with omnidirectional motion flexibility in $x - y - z$ coordinates. Mechanical design steps and forward-inverse kinematics of the robot are derived and presented in [32] as Ph.D work. Therefore

the details of mathematical kinematic model of the robot is beyond the scope of this work.

4.3.2 Experiments and Results

In order to assess the performance of the derived kinematics and the controller some experiments are conducted. The experimental setup is given in Fig.4.11. Here, a low power laser pointer is attached to the end effector of the robot and task space positions in $x - y$ coordinates are measured by means of Position Sensitive Device (PSD) which has $4mm \times 4mm$ detection area. PID controller with disturbance observer is employed to reach desired positioning in task space. Corresponding system responses for both configuration and task space are provided below.

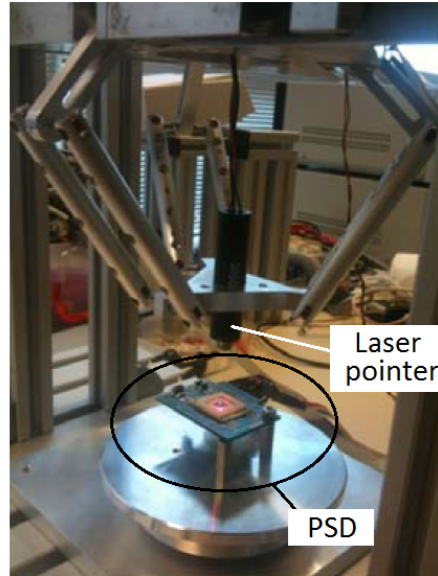


Figure 4.11: Delta robot experimental setup

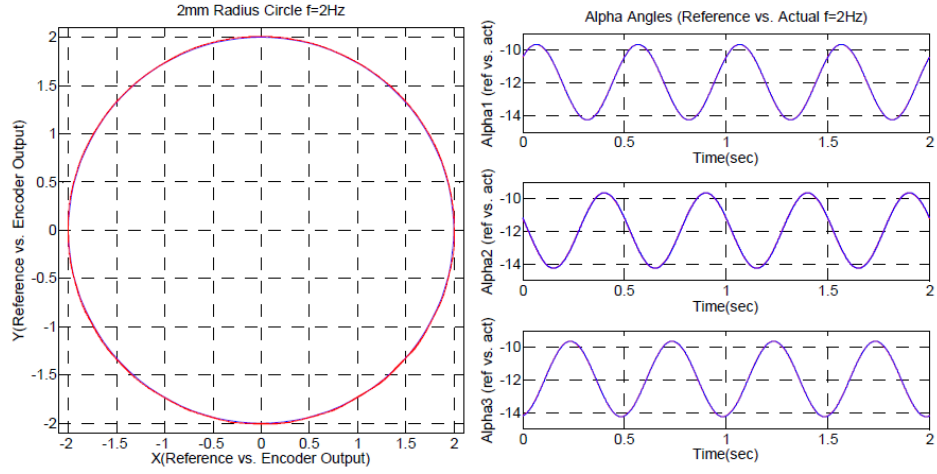


Figure 4.12: (a) 2 mm circle reference ($f = 2\text{Hz}$) (b) Corresponding motor angle ref. vs. actual position

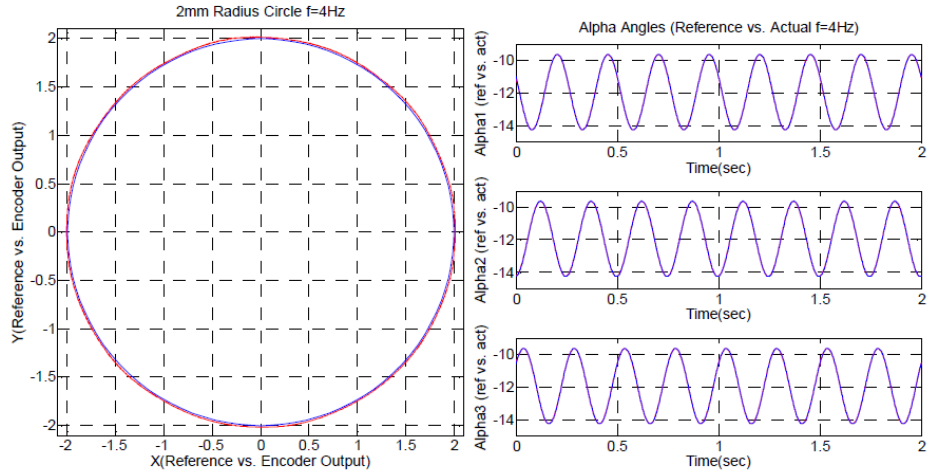


Figure 4.13: (a) 2 mm circle reference ($f = 4\text{Hz}$) (b) Corresponding motor angle ref. vs. actual position

$x - y$ plots for 2 mm circle reference with 2 Hz and 4 Hz frequency and actual positions measured by means of incremental encoders embedded in the actuators are provided in Fig.4.12 and Fig.4.13, respectively. These results validate the accuracy of the proposed controller with precision of approximately $70 \mu\text{m}$

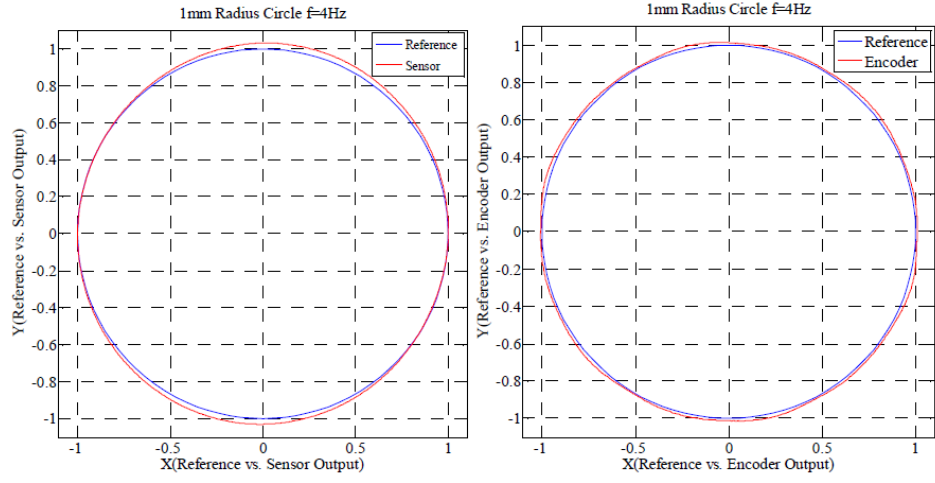


Figure 4.14: 1mm radius $f=4$ Hz circle reference (a) ref. vs. sensor (b) ref. vs. encoder

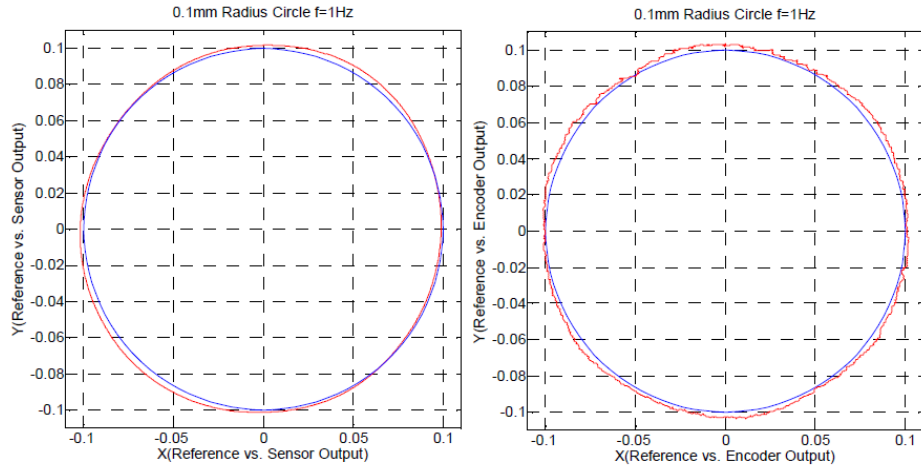


Figure 4.15: 0.1mm radius $f=1$ Hz circle reference (a) ref. vs. sensor (b) ref. vs. encoder

Similarly, tracking of smaller circular references are also tested with the controller as in Fig.4.14 and 4.15. Measurements in configuration space and task space are provided to verify the accuracy of theoretical kinematics of the robot.

4.4 Autofocusing Inspection System

4.4.1 Camera system description

Micro-manufacturing of meso, micro and nano parts requires accurate inspection and detection vision systems. In that sense, the desire to have measurements from a vision unit has been increasing rapidly with the recent developments in small scale robotics applications like micromanipulation or microassembly. CCD cameras integrated to optical microscope systems are usually preferred as the measurement and inspections units for micro level applications due to their simple and cheap nature. They are widely employed for visual feedback of automated cellular micro-injection tasks or micro-manipulation and microassembly of tiny electromechanical parts. These tasks require continuous adjustment of magnification and focus of the vision equipment for precise detection of the edges and measurement of micro part location. In order to attain precise micro part inspection within microfactory concept a new autofocusing microscope setup is designed [33] as shown in Fig. 4.16)

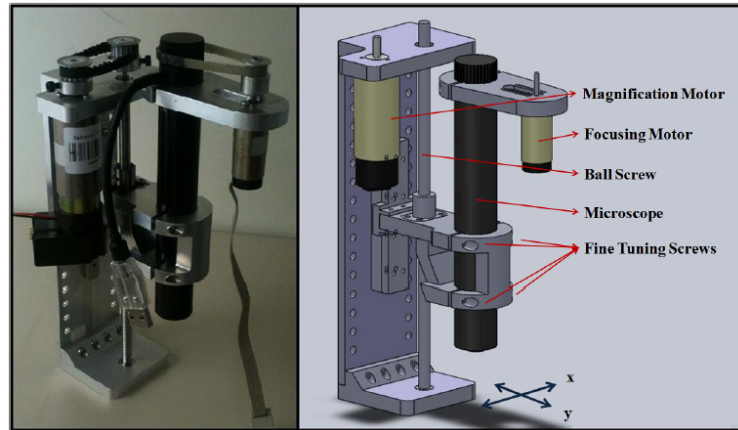


Figure 4.16: Autofocusing camera system

The presented system is small in size in order to fit to microfactory and consist of a miniature TIMM 400 Digital Miniature Microscope. The microscope provides

freedom of focusing by means of adjusting screw to have the desired images with sharp edges. Magnification level of the microscope is primarily related to the distance between the microscope objective and the object to be viewed. Therefore the system has two degrees of freedom thus two DC motors are used to automatically adjust both magnification and focus of the camera. Experiments with this system displayed clear relations between the effect of changing magnification on focus and changing focus on magnification. These relations are analyzed and a self optimizing controller is proposed based on acceleration control framework. The description of the systems mechanical design, the analysis of coupling between magnification and focus, and the mathematical derivation of the self optimizing controller are presented in detail in [Eray's paper] and beyond the scope of this work.

4.4.2 Experimental Results

In order to verify the optimization algorithm, experiments are carried out for testing the robustness of the system against changes in the magnification level. Initially, the camera is focused on an very small image and then a reference position is given to the magnification motor resulting in change of the magnitude of zoom. With the changes in the zoom level, the camera becomes defocused then the focusing algorithm start to run. The results of the experiment are given in in Fig. 4.17) below.

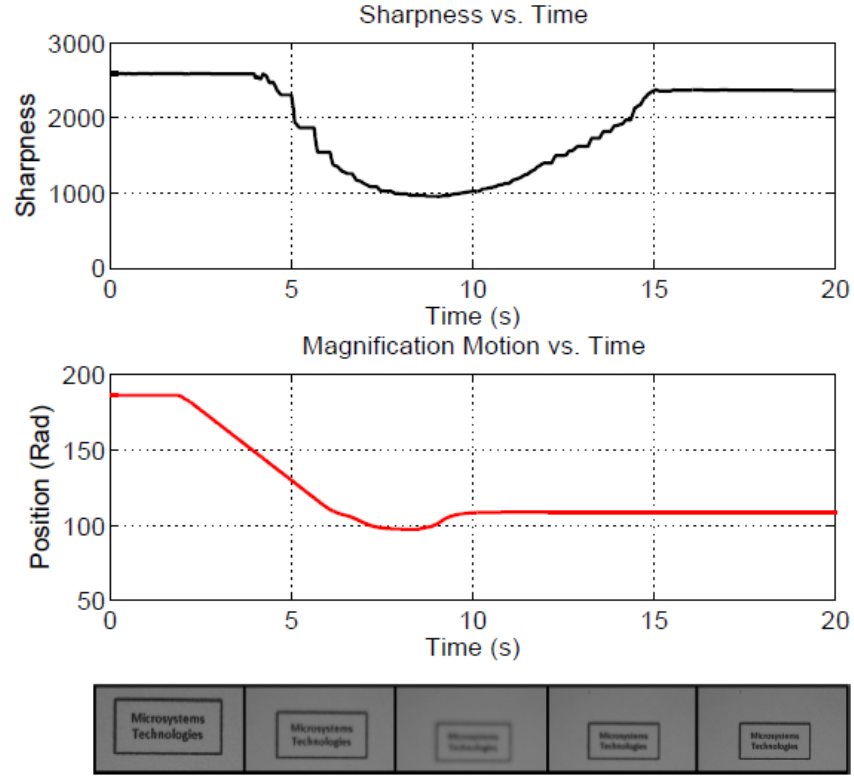


Figure 4.17: Autofocusing experimental results

The first plot shows how the sharpness of a focused system changes with the changes in zooming level and how the proposed algorithm recovers back the focus level. The images taken during this procedure is also given below the plots to provide further insight to the overall process. Initially, the camera is focused at certain magnification level then the camera is slowly raised up resulting in drop in focus and magnification level. Then the algorithms start to run to adjust the focus and magnification to an optimum level. It is obvious from the sharpness plots of the system and from the recorded pictures that the algorithm is robust against the disturbance created by the magnification motor and can track the gradient until the maximum focus point for this level of magnification is recovered.

4.5 Galvanometric Laser Beam Steering System

Micro-machining is crucial for micromanufacturing applications where micro-mechanical cutting, electrochemical (ECM), electrical discharge (EDM) or laser machining techniques are widely used [5]. Main advantage of laser micromachining over other mentioned techniques is it has minimized focus resolution, low heat input and high flexibility of power and beam control. With development of short and ultrashort pulse lasers such as femtosecond lasers it become possible to machine parts with ultra precision [34]. It is due to laser light that consists of photons. They are much smaller than electrons and suitable for very high precision machining applications down to few microns. Laser technology can be used for welding, cladding, ablation, stripping, trimming, cleaning of micro parts, texturing of micro-channels, 3D printing and marking [24]. Two laser machining techniques are widely employed such as synchronised overlay scanning (SOS) with masking and sync scan (SS) by direct write method where laser beam is scanned by mirrors or motion stage [35]. First method is widely used for MEMS fabrication with use of masks that determine the pattern to be machined and aperture describes the depth of the substrate. In direct writing method the laser beam is focused and used for machining purposes where high speed is of main concern. It is flexible since it doesn't require mask and the texture data to be machined can be provided in software program preserving low cost and flexible implementation compared to masking method. The size of a writing pattern is limited to rotational angles of scanning mirrors or the stroke size of a motion stage. Combination of both galvanometric laser beam steering system and motion stage can be also used to increase the writing area [36]. Galvanometric laser beam steering frameworks are widely used for writing 1D images thus single mirror is used for reflection of laser light, or 2D and 3D dimensional patterns can be machined with employment of two or more mirrors [37]. They are also used for laser material microprocessing

[38], medical imaging [39] or marking [40]. By controlling angular position of the motors with attached mirrors in a proper way a desired image can be achieved on the image field. Image is measured and assessed by means of position photodetectors [41]. Minimum rotation angle and size of mirrors determines the resolution of an image and scanning speed [42]. One advantage of galvo scanners over motion stages is their fast scanning speed. Higher resolution means higher amount of data to be processed hence smaller mirrors permit fast processing. Higher data processing for galvos can be achieved by employment of fast computational units such as DSP and FPGA [43]. However larger image size processing may require addition of motion stage. This section presents application of galvanometric laser beam steering system [44] for machining or marking images in micron scale for microfactory. A simple kinematic model of two motors with attached mirrors is derived. Model is tuned and verified for both forward and inverse kinematics by two sensors; position sensitive device (PSD) placed on image field and the optical position sensor (OPS) embedded in the galvo motors. Reference shapes to be tracked are provided as CAD drawings. Drawings are parsed to $x - y$ coordinate points, interpolated and further fed to the system as reference voltages. By implementation of PI controller the angular position of the motors are controlled to minimize laser beam position error on image field [45].

4.5.1 System Overview

Galvo scanner system [44] under consideration in this paper is depicted in Fig. 4.18. Two silver-coated octagon shaped mirrors are attached to galvanometer motors with limited angular travel of $\mp 20^\circ$ mechanical degrees. Its acceleration is directly proportional to the current applied to the stator coils. Current flowing through coils induces flux that turns permanent magnet rotor through an arc. This configuration enables faster response and higher system resonant frequencies compared to rotor

coil configuration. Optical position detector embedded in the system provides motor position information. As the galvos move different amounts of light are detected by photodiodes and the produced current is proportional to motor position. Commercial servo driver boards that include both controller and amplifier circuits is used to drive the actuators. The servo circuit interprets current position of the motors from the position detector then by means of PID controller regulates drive currents of the actuator by positioning them to the desired position and synchronizing. The driver is voltage controlled meaning that applied voltages are proportional to certain degrees of angular rotation. This rotation of the mirrors result in certain motion of the reflected laser ray on image plane. Hence by controlling voltages, control of an image coordinates can be achieved on $x - y$ plane.

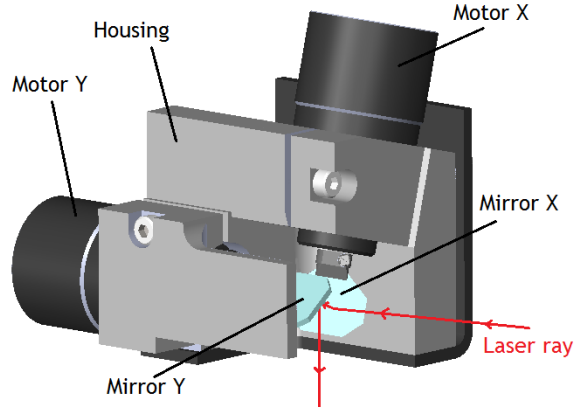


Figure 4.18: Galvo laser beam scanning system

4.5.2 Kinematics of the system

For precise marking laser beam should be guided accordingly to draw desired image on the surface of a specimen. In order to find the relation between the angular positions of the mirrors that correspond to applied voltages and the position of reflected laser spot on image field, a kinematic model should be derived. Theoretical model based on the geometry of the reflected laser beam is presented in [46,47]. However these models

are based on ideal assumptions. In practical implementation for micro-positioning the position of the beam on $x - y$ plane greatly sensitive to the size of the mirrors, orientation of the laser light source, distance between two mirrors, distance from the sample of interest and imperfection in drive electronics. The relation between applied voltage and the optical angle of reflected light should be determined with minimum error for accurate positioning on image field. For this purpose parameters of transformation from configuration space to image space should be tuned in order to achieve the best performance. Fig. 4.19 demonstrates the geometry of laser light reflection and effect of galvos rotation on the beam reflected to the $x - y$ image plane.

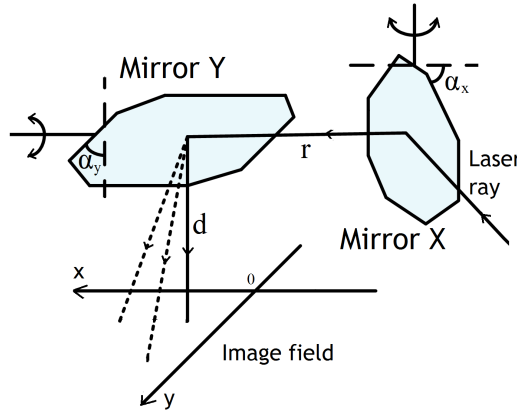


Figure 4.19: Laser beam reflection geometry by means of galvo mirrors

The laser ray first hits the mirror X, reflected light further hits the mirror Y and finally appears on image field as a spot. When mirror X or mirror Y are rotated the beam moves in x or y direction on $x - y$ coordinate plane, respectively. Then the relation between optical angles and $x - y$ coordinate points can be expressed as follows

$$x = (r + \sqrt{d^2 + y^2}) \tan \theta_x \quad (4.3)$$

$$y = d \tan \theta_y \quad (4.4)$$

Here, x and y are coordinates of beam position on image field, θ_x and θ_y are optical rotation angles of mirrors, r and d are the distance between mirrors and the distance from mirror Y to image field respectively. According to vendors specifications applied voltage to the galvos is half of mechanical rotational angle where mechanical angle is proportional to optical angle. Then this relation can be expressed as follows

$$V_x = \frac{1}{2}\alpha_x = K_x\theta_x \quad (4.5)$$

$$V_y = \frac{1}{2}\alpha_y = K_y\theta_y \quad (4.6)$$

Here, K_x and K_y are scaling constants due to commercial driver input voltage to output mirror angle relations. Then substituting Eq. 4.5 and Eq. 4.6 into Eq. 4.7 and Eq. 4.8 a following voltage to scalar coordinate points relation can be obtained

$$x = (r + \sqrt{d^2 + y^2}) \tan\left(\frac{V_x}{K_x}\right) \quad (4.7)$$

$$y = d \tan\left(\frac{V_y}{K_y}\right) \quad (4.8)$$

given $x - y$ reference coordinates of the desired image the required voltages can be calculated by inverse transformation of the relation given in Eq. 4.7 and Eq. 4.8

$$V_x = K_x \arctan\left(\frac{x}{r + \sqrt{d^2 + y^2}}\right) \quad (4.9)$$

$$V_y = K_y \arctan\left(\frac{y}{d}\right) \quad (4.10)$$

When reference points x^{ref} and y^{ref} of the desired shapes are provided by the user the reference voltages V_x and V_y are generated and fed to the system to achieve the desired position on image plane. Fig. 4.20 and Fig. 4.21 present simulation results for

the model given above. Here, voltage is applied between $V_{min} = -10V$ and $V_{max} = 10V$ due to driver limitations and corresponding x and y coordinates are plotted. For simplicity parameters are chosen as $K_x = K_y = 0.25$. Since applications in microfactory consider image sizes in microns and few millimeters the range of interest is taken between $V_{min} = -2V$ and $V_{max} = 2V$ as labeled with rectangular regions with dashed lines. In this regions the system has approximately linear behavior.

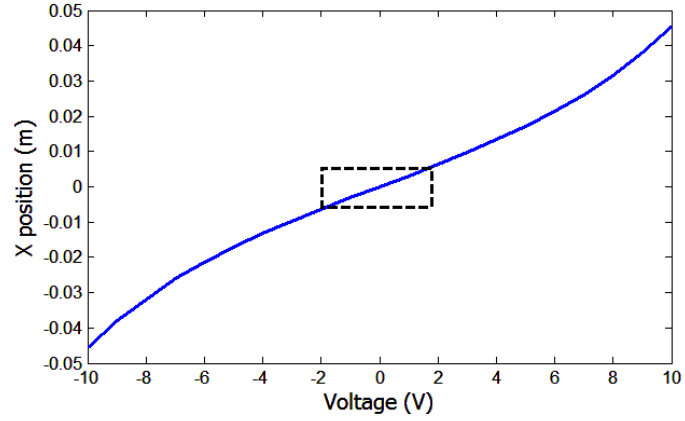


Figure 4.20: System behavior in x coordinate

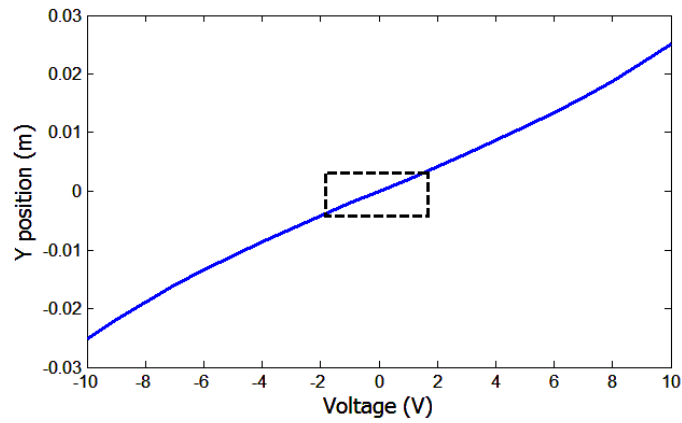


Figure 4.21: System behavior in y coordinate

The actual model can be determined by measuring positions on image plane and by tuning K_x and K_y parameters actual positions can be matched with the reference

positions. Once the model is tuned offline, further fine positioning with employment of controller additional compensation of errors online can be achieved.

4.5.3 Reference image generation

The overall system block diagram is depicted in Fig. 4.22. One advantage of the current approach is the ease and flexibility of reference image generation. Flexibility of desired image generation to be marked or machined is crucial especially in industrial applications where user doesn't have to constrain him/herself with fixed images to be machined. Instead user should be simply able to draw any demanded pattern as CAD drawing. For this purpose coordinates of the desired output image for a galvo scanning system are generated from CAD drawing with implementation of coordinate points parsing algorithm on MATLAB. Before parsing, the desired image to be marked or machined should be saved as any 2D CAD file in *dxf* format. The parsing algorithm reads *dxf* file line-by-line and determines the geometry of the input shape as circle, line or etc. When appropriate shapes are detected that match any shape in program library equally spaced data points are fitted through the entire path of the pattern and stored as vectors. By means of interpolation algorithm more points are fitted in between the parsed data points in order to obtain more accurate shape. Generated x and y coordinate points are further extracted as arrays in C code by implementation of MATLAB *fopen* and *fprintf* functions. C file is then included as reference input data file to the system.

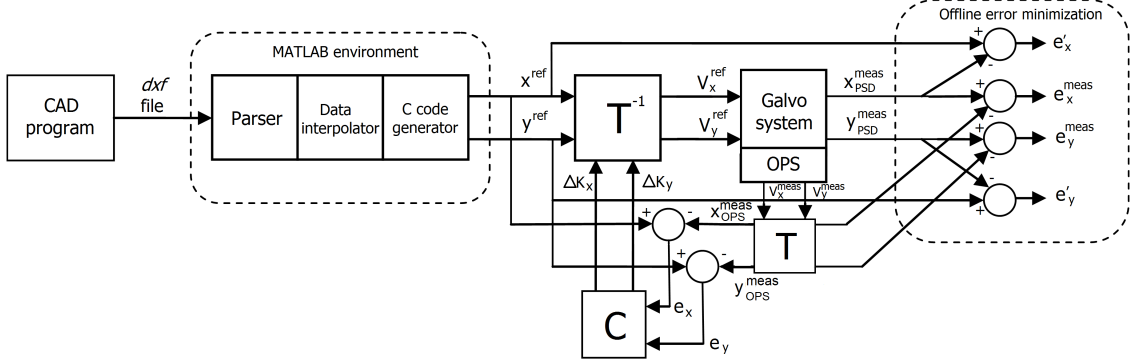


Figure 4.22: Overall system block diagram

4.5.4 Model tuning and verification

In order to satisfy accuracy in positioning both in configuration space and image space one should guaranty that the model is valid for both forward and inverse transformations. To achieve accurate response of the system the derived model is tuned by alteration of K_x and K_y parameters of the kinematic equations that are in turn proportional to voltages applied to the system. The model is tuned offline by manually matching x_{PSD}^{meas} and y_{PSD}^{meas} positions measured by position sensitive device (PSD) placed on image field with those of reference data points x^{ref} and y^{ref} supplied to the system. Optical position sensor (OPS) embedded in galvo motors is used to measure angular positions of the galvo motors as voltage values V_x^{meas} and V_y^{meas} . Measured voltages can be used to obtain x_{OPS}^{meas} and y_{OPS}^{meas} points by forward transformation equations given by Eq. 4.7 and Eq. 4.8 and then compared with x_{PSD}^{meas} and y_{PSD}^{meas} (see Fig. 4.23). Therefore by minimizing the errors e'_x , e'_y , e_x^{meas} and e_y^{meas} the system model approaches to more accurate form. Since PSD device placed on image plane has to be removed for operations where high power laser is considered for machining and marking, online minimization of the errors in x and y become infeasible without PSD data. Therefore model tuning is performed manually. For further online control applications OPS is suitable for position feedback to compensate errors.

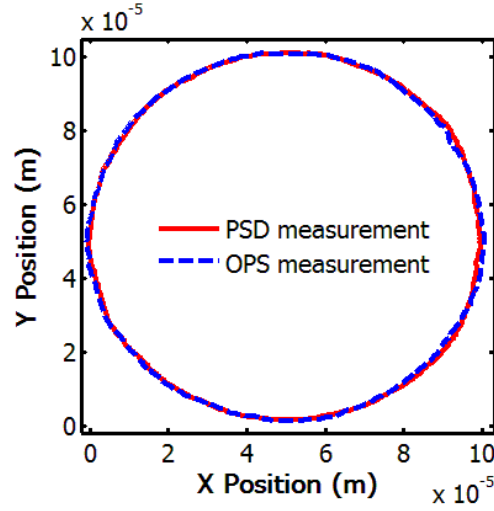


Figure 4.23: 100 μm circle PSD to OPS measurement plot

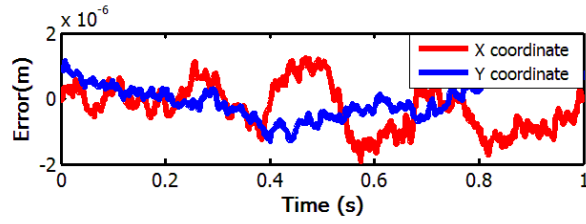


Figure 4.24: 100 μm circle PSD to OPS measurement error plot

Plots measured at configuration space and image field are given in Fig.4.24 to verify validity of both forward and inverse models with errors within 2% of the desired shape.

4.5.5 Controller approach

For online applications the main goal is to compensate positioning errors e_x and e_y by appropriately regulating input voltages. For this purpose the inverse transformation equation is modified as

$$V_x = (K_x + \Delta K_x) \arctan\left(\frac{x}{r + \sqrt{d^2 + y^2}}\right) \quad (4.11)$$

$$V_y = (K_y + \Delta K_y) \arctan\left(\frac{y}{d}\right) \quad (4.12)$$

here, ΔK_x and ΔK_y are the regulation variables. These variables are result of the controller. Since the galvo system has a linear behavior between inputs and outputs a simple PI control method can be employed to achieve error compensation. Then the controller is expressed mathematically as follows

$$e_x = x^{ref} - x_{OPS}^{meas} \quad (4.13)$$

$$e_y = y^{ref} - y_{OPS}^{meas} \quad (4.14)$$

then

$$\Delta K_x = K_{px}e_x + K_{ix} \int e_x dt \quad (4.15)$$

$$\Delta K_y = K_{py}e_y + K_{iy} \int e_y dt \quad (4.16)$$

Here, e_x and e_y are the errors in x and y position on image plane, x, y^{ref} are the reference coordinates and x, y_{OPS}^{meas} are the measured points by optical position sensor. $K_{px,y}$ and $K_{ix,y}$ are the proportional and integral controller gains.

4.5.6 Experimental results

Experimental setup is depicted in Fig. 4.25 to assess the system for positioning. It consists of galvanometric laser beam scanner system, low power laser pointer and position sensitive device placed under the system. Two mirrors reflect the laser ray coming from side to the image field where the PSD is placed. PSD has $4mm \times 4mm$ sensitive area with detection resolution of $1\mu m$. The sensor is separated into four

quadrants thus enabling both positive and negative $x - y$ coordinates. dSPACE 1103 is used as a RT controller unit and the galvo drivers are employed to drive the motors. For experiments an ordinary laser pointer is chosen to avoid PSD damage. 2D images are drawn on Microsoft Office Visio 2007 software program and saved in *dxf* file format. The file is further parsed, interpolated and saved as C code. Voltage references are calculated and fed to the system. Position measurements are taken by calibrated optical position sensor and experimental results are presented below.

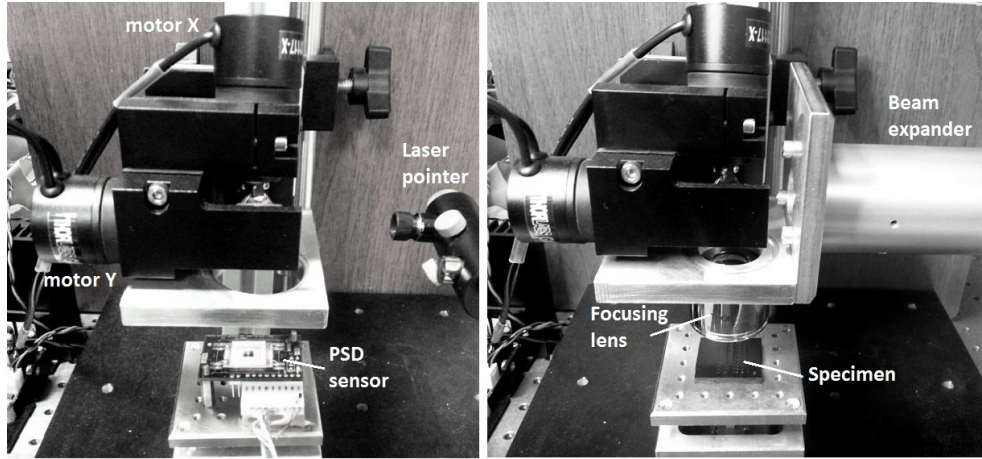


Figure 4.25: Galvo experimental setup

System response with PI controller for $250\ \mu\text{m}$ and $50\ \mu\text{m}$ radius circle reference is provided in Fig. 4.26 and Fig. 4.28. Error plots for these references demonstrate that inaccuracies are in the range of less than 2%.

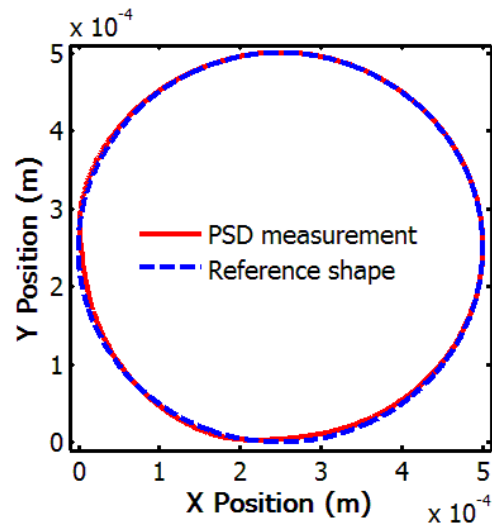


Figure 4.26: 250 μm radius circle reference tracking response

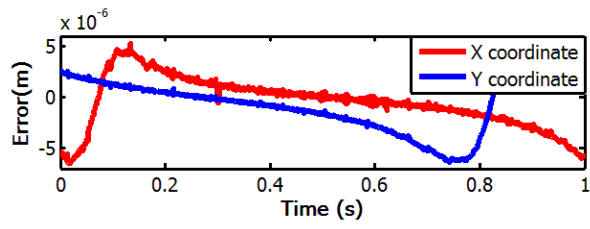


Figure 4.27: 250 μm radius circle reference tracking error

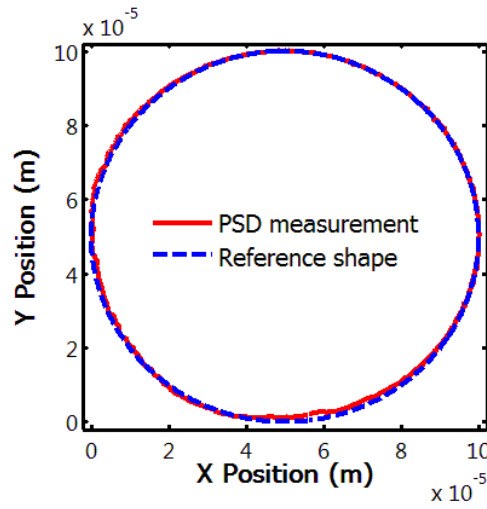


Figure 4.28: 50 μm radius circle reference tracking response

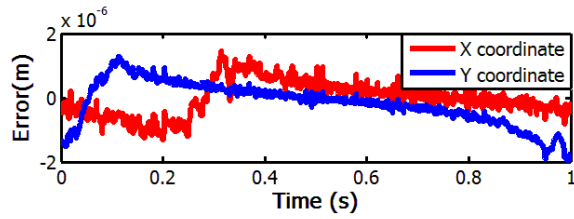


Figure 4.29: 50 μm radius circle reference tracking error

For assessing the system behavior for sharp edges a rectangular reference shape is drawn as letter "G" as depicted in Fig. 4.30 and Fig. 4.32. For these references system has errors also within 2%.

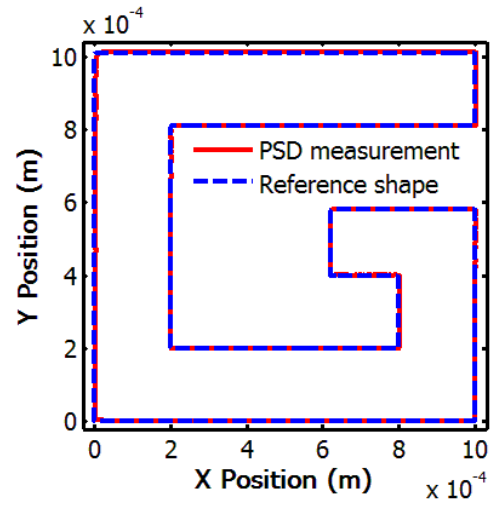


Figure 4.30: 1 mm size rectangular "G" letter reference tracking response

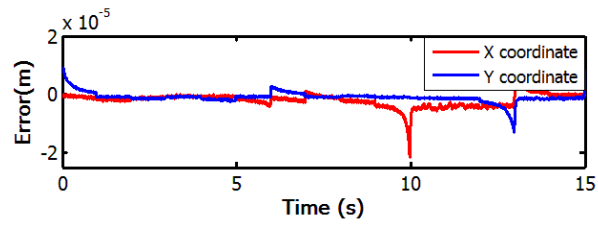


Figure 4.31: 1 mm size rectangular "G" letter reference tracking error

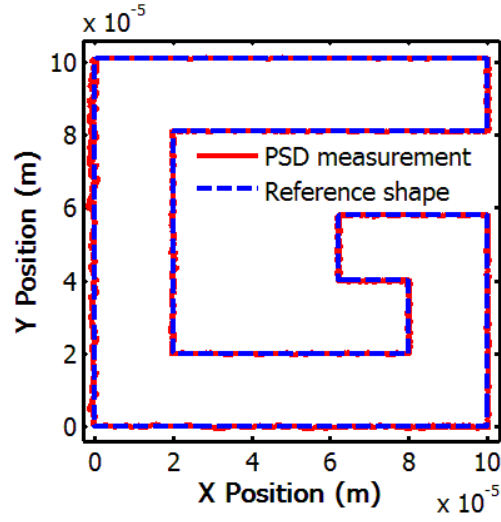


Figure 4.32: 100 μm size rectangular "G" letter reference tracking response

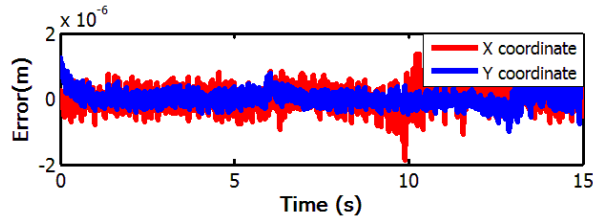


Figure 4.33: 100 μm size rectangular "G" letter reference tracking error

For assessment of the system in real marking applications, a 100 W laser with 25 KHz pulsed light configuration is used. Beam is focused by means of focusing lens and directed to anodized coated black aluminum substrate. The marked results for circles and letter "G" are provided in Fig. 4.34 and Fig. 4.35 respectively.

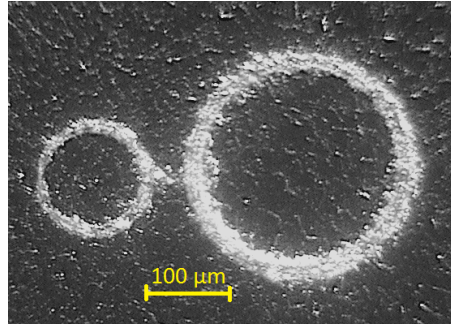


Figure 4.34: 50 μm and 150 μm radius marked circles

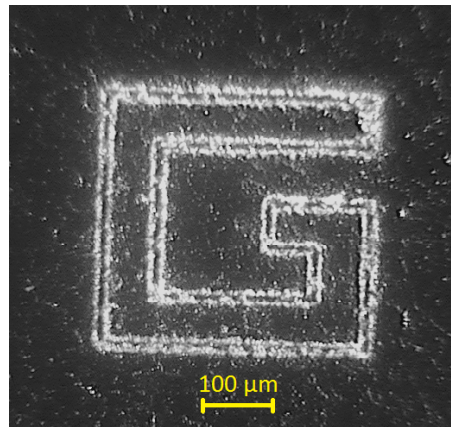


Figure 4.35: 400 μm marked rectangular letter "G"

4.6 High precision positioning stage

With miniaturization of devices and high precision positioning systems in various fields, fine positioning become crucial. For this purpose several researches are devoted to design reliable and precise actuators for last two decades. Though electromagnetic actuators are common positioning devices they lack high precision, suffer from high hysteresis, backlash and low stiffness. For this reason piezoelectric actuators become advantageous for their high precision, low power consumption, high stiffness and higher stall force to size ratio characteristics. Nowadays a demand for such actuators arises in various fields including medical, industrial and aerospace applications where fine positioning is of main concern. Positioning in micro and nano scales requires careful examination of the system and application of relevant control techniques. Piezoelectric motors proved to be compatible in MRI scanner applications where traditional electromagnetic actuators are prohibited because of electromagnetic field interactions that effect functionality of the MRI system [48]. They can be effectively employed in AFMs where stationing of a specimen in nanometers is required [49]. Piezoelectric actuators are generally integrated to fine precision positioning stages. Translation stages with piezoelectric actuators can be exploited in single DOF positioners [50-52] or multiple DOF positioning [53-55]. Since piezoelectric actuators are non-linear and inherit hysteresis their control become difficult. Hysteresis can be overcome by applying compensation techniques to linearize the system first and implement linear controllers such as PID to improve positioning accuracy [56]. Hysteresis can be also modeled as Duhem [57], Prandtl-Ishlinskii [58] or Preisach [59] models and by designing proper controllers desired accuracy can be achieved. Several control techniques are proposed to improve the tracking error in literature such as fuzzy controller [60], repetitive controllers [61,62] or repetitive control augmented with non-linear PID controller [63]. Feedforward control with PID gain scheduling

for walking PiezoLEGS motor [64] is presented in [65,66]. In this approach overshoots are significantly improved by varying amplitude and phase of the waveforms with overlapping trajectories. Since phase and amplitude of the actuator is related to the step size [67], by modulating these parameters step size control can be achieved. Authors proposed an adaptive controller scheme for step size control by changing amplitude and phase shift between sinusoidal waveforms to improve positioning precision and overshoots. Polynomial controller for the same type of motor that involves velocity polynomial function according to position error and step size is introduced in [68]. Here, similarly velocity of stepping and step size is varied with approaching to desired position to improve overshoots. Authors also proposed a bang-bang controller method applied to nano-robotic positioning stage [69]. Optimal control methods such as Simple Genetic Algorithm (SGA) is also employed for fine positioning [70]. Walking piezoelectric motor is modeled and simulated in [71]. Based on the model optimal driving waveforms are derived that improve the driving properties of the motor. This section presents micro/nano-metric positioning control of a piezo-walker [64] in both discontinuous and continuous modes. Static and dynamical models of the legs are derived. Some identification experiments are conducted to verify the models. Based on identifications controllers for both modes of operation are designed. These approaches result in positioning accuracy of the motor down to micro and nanometers.

4.6.1 Walking piezoelectric motor

Linear quasi-static PiezoLEGS motor is depicted in Fig. 4.36. It is a miniature piezoelectric linear motor with direct drive-backlash free, quick response and high speed operational characteristics. operating on walking principle of piezoelectric bimorph legs. Walking operation of four legs exerts force on the drive rod which results in high

precision linear motion of the rod (see Fig. 4.37) down to micro-nano-meters. Single bimorph leg consists of two electrically insulated stacks of piezoelectric material. Application of two independent drive voltages to both stacks results in elongation or bending of the whole leg. This elongation and bending causes movement of the leg tip in certain trajectory. Tip trajectory of motion varies with applied waveforms, for instance, application of sinusoidal waveforms with certain phase shift results in elliptical trajectory movement of the leg tip. Driving waveforms can be controlled by varying amplitude, phase and frequency. Waveform amplitude and phase difference correspond to step size, and frequency is proportional to the speed of stepping [67].

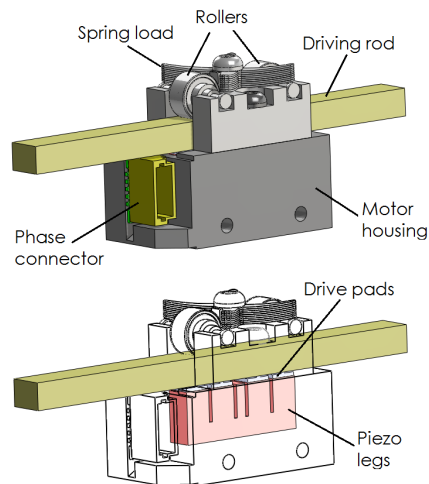


Figure 4.36: PiezoLEGS motor structure

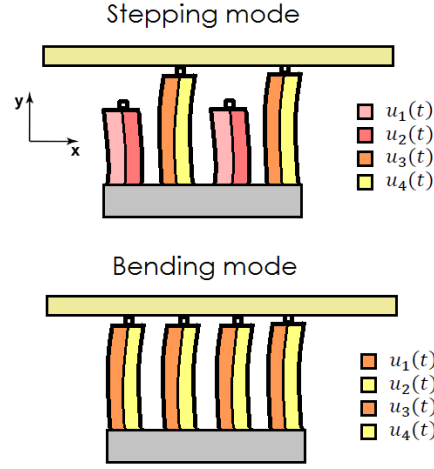


Figure 4.37: Principles of motor operation in stepping and bending modes

The motor can be driven in two modes: stepping mode and continuous mode. In stepping mode legs are not continuously in contact with the rod thus they operate in walking manner as depicted in Fig. 4.37. Legs are driven in pairs of two meaning that always two of the legs are in contact with the driving rod until other two legs acquire the rod. In continuous mode, all four legs are in clamping contact with the drive rod never losing contact. Motion is a result of bending action of the legs. This allows the highest precision in positioning down to few nano-meters.

Piezoelectric legs are driven by application of positive voltages with amplitudes up to 46V. Sum of voltages applied to the two piezo stacks of one leg causes the leg to elongate and the difference causes it bend. Mathematical model describing deflection and elongation of piezoelectric bimorph is given by Eq. 4.17 and 4.18 [17]. Equations are derived using basic mechanics principles of static equilibrium and strain compatibility between layers of bimorph. The model is developed on the basis of inverse piezoelectric effect and Euler-Bernoulli theory of elastic deformation. The leg is considered as a cantilever beam and only forces generated by inverse piezoelectric effect are included and the steady state deflection and elongation can be given by

$$x = \underbrace{\frac{3d_{33}L^2}{4tD}}_{K_1}(u_1 - u_2) \quad (4.17)$$

$$y = \underbrace{\frac{d_{33}L}{2t}}_{K_2}(u_1 + u_2) \quad (4.18)$$

Here, x and y are the deflection and elongation of the legs respectively, d_{33} is piezoelectric charge constant, L is the length of leg, D is the half width of the leg, t is the thickness of piezoelectric layer, u_1 and u_2 are the driving voltages applied to the stacks.

Different waveforms are used to drive bimorph piezoelectric actuators. In turn, the waveforms themselves can be varied in various ways. For the movement to be as smooth and accurate as possible, it is desirable to control the frequency, amplitude, and phase of the waveforms supplied to the piezoelectric legs. This gives the most freedom in the control of the movements of the different legs. For instance, application of sinusoidal voltages results in elliptical motion of the leg tip. Phase difference between waveforms and amplitude defines step size and frequency sets speed of walking [66].

4.6.2 Operation in discontinuous mode

In stepping or in discontinuous mode, legs are driven in pairs of two meaning that always two of the legs are in contact with the driving rod until other two legs acquire the rod back. In this configuration, legs imitate running action on the rod surface when periodic positive voltages are applied. This continuous step on and push actions enables rod motion in horizontal axis. The speed of motion can be adjusted by changing frequency of the periodic signals.

Static relationships between applied voltages and the leg tip trajectory of movement

are now used to derive the dependence of step size on amplitude and phase difference of the driving voltages applied to two stacks of a single leg. Since driving legs should be moving in a form of closed periodic trajectory to achieve motion, applied voltages can be defined as:

$$u_1(t) = \frac{A}{2}(1 + \sin(\omega t)) \quad (4.19)$$

$$u_2(t) = \frac{A}{2}(1 + \sin(\omega t + \varphi)) \quad (4.20)$$

$$u_3(t) = \frac{A}{2}(1 + \sin(\omega t + \pi)) \quad (4.21)$$

$$u_4(t) = \frac{A}{2}(1 + \sin(\omega t + \pi + \varphi)) \quad (4.22)$$

Voltages u_1 and u_2 are applied to one pair of the legs and voltages u_3 and u_4 to other pair. There should be always a phase shift of π radians between the pair of phase voltages in order to guaranty contact of at least one pair of the legs and the rod. For instance, to generate elliptical trajectory of motion of the leg tip in $x - y$ plane one pair moves through the upper half of the ellipse the other pair moves along lower path then till they switch in between. This switching or stepping behaviour is repeated periodically. In order to define step size it is enough to use only one pair of voltages u_1 and u_2 . The leg tip trajectories of motion for different phase values (φ) and amplitudes (A) are depicted in Fig. 4.38. Since for this motor the effective motion is performed in x coordinate therefore step size σ depends on difference between x_{min} and x_{max} . They are the extreme values of the function $x(t)$ which specifies the motion in x plane. Then the dependence of the step size on amplitude and phase can be expressed as

$$x_{max} = K_1 A \sin\left(\frac{\varphi}{2}\right) \quad (4.23)$$

$$x_{min} = -K_1 A \sin\left(\frac{\varphi}{2}\right) \quad (4.24)$$

$$\sigma = 2K_1 A \sin\left(\frac{\varphi}{2}\right) \quad (4.25)$$

σ in Eq. 4.25 is amplitude and phase dependent, and frequency independent. Frequency of the driven voltages defines velocity of motion of the rod. In other words, it defines number of elliptic trajectories (i.e. number of steps) that leg tip makes in a period of time.

Elliptical trajectories of a leg tip movement ($x(t)$ vs $y(t)$ plot) with different phase shifts and a half amplitude is depicted in Fig. 4.38. It can be easily noticed that step size is highly dependent on amplitude and phase variations.

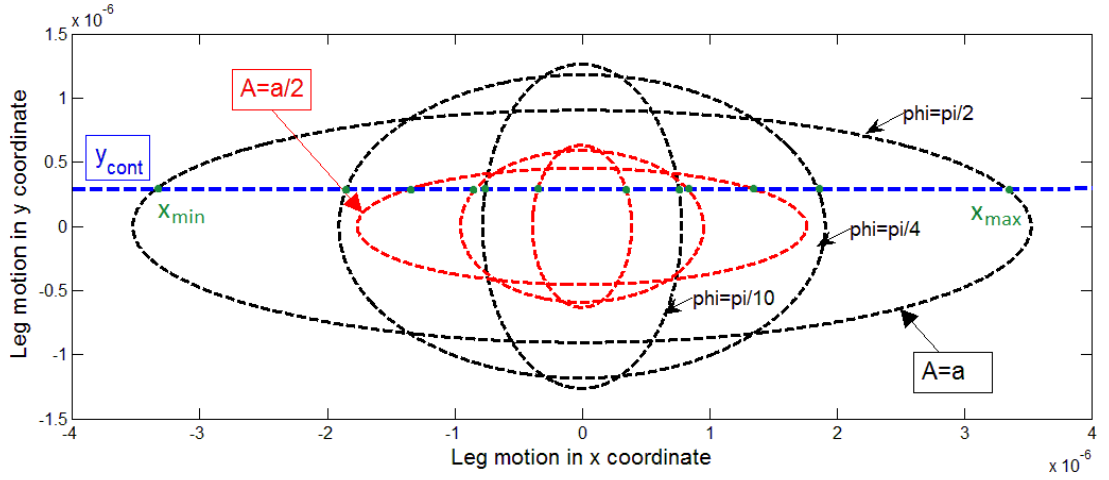


Figure 4.38: Legs tip trajectory with varied phases (black) and a half amplitude (red)

It is important to note that the rod motion will be possible only if there is enough force generated by the legs in the vertical direction. The force generated in the vertical direction has to be sufficient to counteract preload force applied to the rod by preload springs. It is important that this condition for the motion is true only when the actuator is not loaded by an external force. The normal force at the tip

of the leg depends on the elongation of the leg's tip in vertical direction y_{con} where they are in contact with the rod denoted as a blue dashed line in Fig. 4.38. If normal force is too small then there may occur a slip between the leg tip and the rod thus motion is uncertain and the control of step size is out of question. Therefore the y_{con} is a certain threshold to be overcome in order to further perform a desired step in x dimension. The upper part of the intersection of this line with the elliptical function of leg movement guarantees the motion of the rod in x plane. Measurement results reveal that driving voltages with low amplitudes cannot move the rod since too low forces are produced by the legs in vertical direction. Maximum elongation can be found as a maximum peak of the elliptical function $y(t)$ and its extreme values are

$$y_{max} = K_2 A (1 + \cos(\frac{\varphi}{2})) \quad (4.26)$$

$$y_{min} = K_2 A (1 - \cos(\frac{\varphi}{2})) \quad (4.27)$$

4.6.2.1 Experimental verification of step size to applied voltage dependence

In order to observe step size dependence on amplitude and phase variation some experiments are performed. The results are given below. Analytical relationships are derived by basic curve fitting technique. Relation between frequency and the rod velocity is also analyzed. For establishing dependence of amplitude on step size, amplitude of the applied waveforms is varied while frequency and phase shift are kept constant ($f = 200$ Hz and $\varphi = 90^\circ$) and result is provided in Fig. 4.39 confirm that there is no rod motion exist until some amplitude value or in other words normal force is exerted. Linear approximation of the dependence between step size and amplitude (A), in the where rod motion exists can be derived as in Eq. 4.28, with amplitude given in (V) and step size in (nm).

$$\sigma = 119.26A - 965.53 \quad (4.28)$$

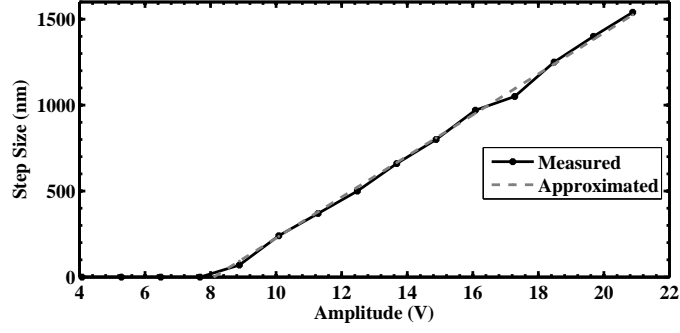


Figure 4.39: Amplitude to step dependence plot

Similarly, dependence between phase difference of applied waveforms and step size is established experimentally. Here the phase shift is varied and both amplitude and frequency are kept constant ($f = 200$ Hz and $A = 20.88$ V). Results are shown in Fig. 4.40. Linear approximation of the dependence between step size and phase shift φ is given analytically in Eq. 4.29, with phase shift in degrees and step size in nanometers.

$$\sigma = 17.02\varphi + 69.95 \quad (4.29)$$

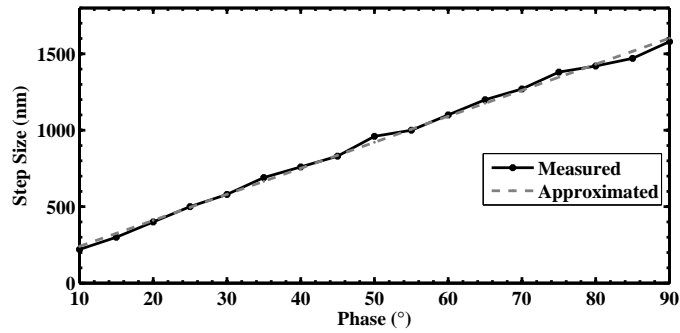


Figure 4.40: Phase shift to step dependence plot

Finally, the relationship between frequency of driving voltages and the rod velocity are derived. In this experiment amplitude and phase shift are assumed to be constant ($A = 20.88$ V and $\varphi = 90^\circ$). Measurement results are depicted in Fig. 4.41. Velocity is calculated as a step size divided with half period of sine signal since one pair of the legs generates effective motion during half period of the sine signal. It must be noted that step size shows negligible variations to frequency change. Therefore average step size is found to be 1546nm . Linear approximation of frequency (f) to velocity (v) plot can be expressed as in Eq. 4.30. Here, frequency is given in (Hz) and velocity in (nm/s).

$$v = 2880f - 113690 \quad (4.30)$$

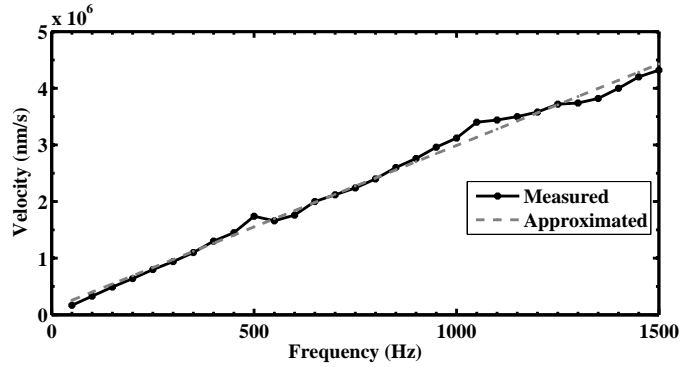


Figure 4.41: Frequency to velocity dependence plot

4.6.2.2 Adaptive Controller Design

Using the information regarding step size dependence on amplitude and phase shift, an adaptive position controller has been designed to accurately position the actuator in stepping mode. The purpose of the controller is to control step size according to absolute error value. Thus the step size is varied with actual position approaching to the reference position. Steps are categorized into two modes so called macro- and

micro-stepping modes. Macro-stepping region is assumed to be far away from the final reference position value. In this region legs move with bigger and faster steps until a certain micro-stepping region is crossed. In micro-stepping region since the magnitude of an absolute error reaches certain small value (mode border), legs move with smaller steps and slower velocity in order to catch the desired position precisely with no overshoot. This approach is called as a step size modulation.

In macro-stepping mode position of the actuator is controlled using cascaded P-PI controller that is based on position and velocity feedbacks. Due to linear relationship between step size and both amplitude (Eq. 4.28) and phase of the driving voltages (Eq. 4.29), maximum possible step can be achieved by keeping amplitude and phase shift at their maximum possible values. Piezoelectric actuator is driven with the sinusoidal waveforms given in the Eq. 4.19 through Eq. 4.22, and the output of the controller is an integral of the frequency multiplied by a constant, i.e. $\omega(t)$. The controller is defined by the following set of equations

$$e_p = x^{ref} - x^{meas} \quad (4.31)$$

$$e_v = K_{pp}e_p - v^{meas} \quad (4.32)$$

$$f = K_{vp}e_v + K_{vi} \int e_v dt \quad (4.33)$$

and

$$\omega(t) = 2\pi \int f dt \quad (4.34)$$

As already mentioned the micro-stepping mode is defined based on the magnitude of the absolute error in position. Absolute error decreases due to the action of the controller. When its value reaches the predefined limiting value, thus $|e_p| < e_{lim}$, amplitude and phase of the driving voltages are modulated according to the Eq. 4.36 and Eq. 4.35 also demonstrated graphically in Fig. 4.42 and Fig. 4.43, respectively.

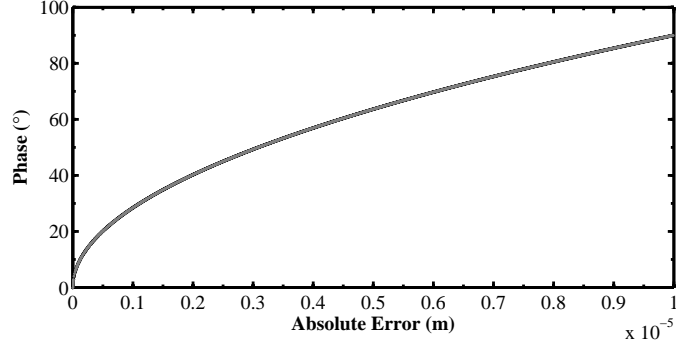


Figure 4.42: Frequency to absolute error plot

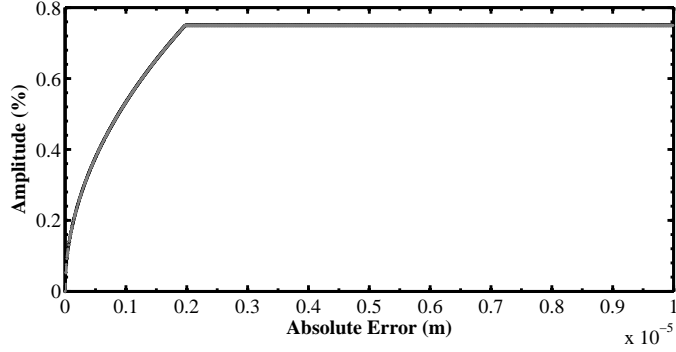


Figure 4.43: Amplitude to absolute error plot

Phase changes slowly dropping from its maximum value to 0 for very small values of the absolute error - no movement of the legs. Amplitude is modulated after the phase reaches some predefined value φ_{lim} . Actuator's step size decreases as the absolute error decreases to settle down to zero when absolute error reaches the vicinity of zero. Linear controller action is not explicitly changed by new formulation and stays the same as defined in the Eq. 4.31 through Eq. 4.34. The phase and amplitude modulations as functions of absolute error are given as

$$\varphi = \varphi_{max} \sqrt{\frac{|e_p|}{e_{lim}}} \quad (4.35)$$

$$A = \text{sat}\left(\frac{A_{max}}{\varphi_{lim}}\varphi\right) \quad (4.36)$$

where maximum and minimum values of the phase and amplitude are bounded to known values. Function $\text{sat}()$ in Eq. 4.36 limits amplitude to its maximum value, if $\frac{A_{max}}{\varphi_{lim}}\varphi$ exceeds it. Overall control system structure is given in Fig. 4.44

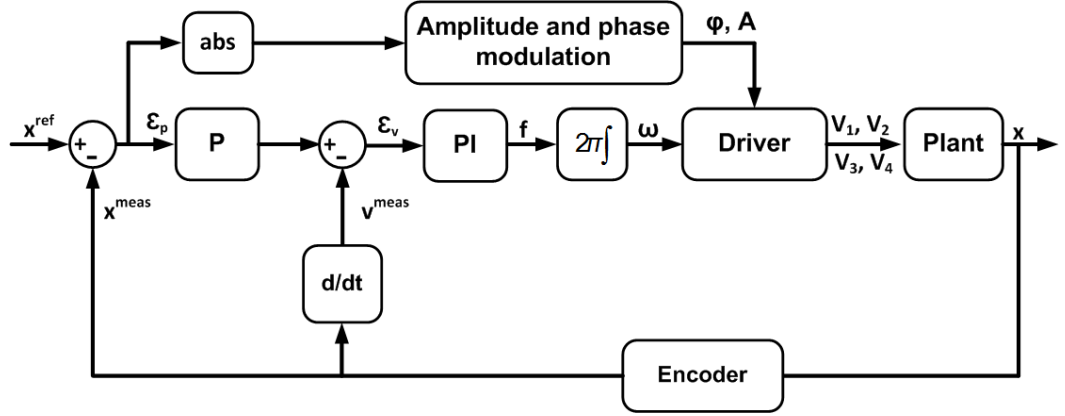


Figure 4.44: Adaptive controller scheme

4.6.2.3 Piezo walker driving electronics design

As mentioned before different waveforms are used to drive bimorph piezoelectric actuators. In turn, the waveforms themselves can be controlled in various ways. For the movement to be as smooth and accurate as possible, it is desirable to adjust the frequency, amplitude, and phase of the waveforms supplied to the piezoelectric legs. Most of the digital micro-controllers are able to generate desired waveforms, however they are not capable of providing high voltages or currents to drive actuators. The motor under consideration in this work can be driven by four phase voltages with variable frequency, amplitude and phase shift. Though it draws low current in the range of few mAmps, the voltage that should be applied is up to 46 V that is not feasible with today's micro-controller electronics. Therefore a need for intermediate amplifier electronics arises.

Initially, a commercial amplifier PDA 3.1 [72] is employed to drive the motor (see Fig. 4.45). This product is developed by the same company PiezoMotor Uppsala (Sweden) AB for this particular actuator. It operates at 12 V DC and produces four phase shifted trapezoidal waveforms to drive four legs. It embeds microcontroller inside that proportionally relates applied input analog voltage to frequency of the output waveforms. Frequency which is directly related to the speed of motor can be adjusted by supplying analog voltage reference to An pin between 0-9.6 V. Hence, the frequency of the output trapezoidal waveforms is an only controllable parameter for positioning application. In addition, microcontroller decides on mode of operation: stepping or bending mode based on control analog voltage level.



Figure 4.45: Commercial driver PDA 3.1

The main disadvantage of this driver is inflexibility in adjusting desired or optimized shape of the waveforms for high precision applications. It results in limited performance characteristics. For this reason in order to gain flexibility in control of applied waveforms two driving circuits are developed; first generation analog voltage amplifier [73] and second generation half bridge switching converter [74] depicted in Fig. 4.46. and Fig. 4.47, respectively.

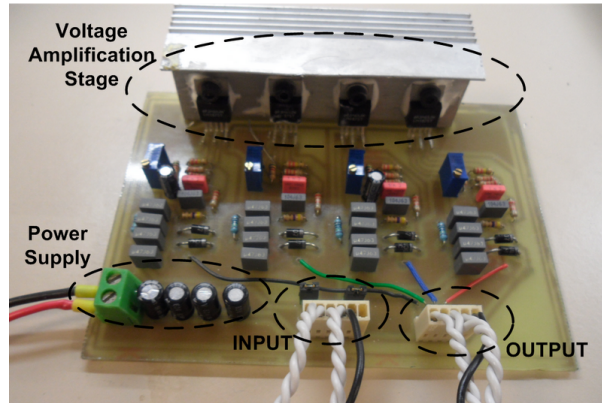


Figure 4.46: Analog voltage amplifier board

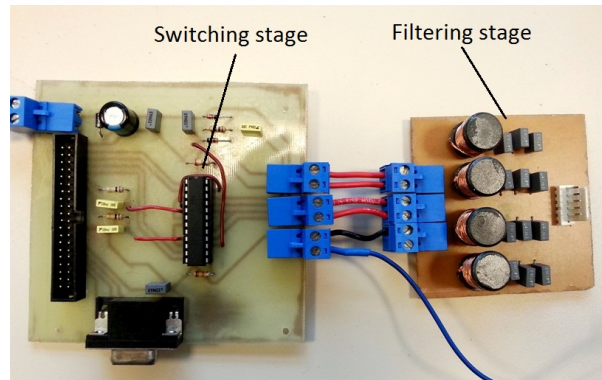


Figure 4.47: Half bridge switching converter board

Central component of the voltage amplifier is a 20 W audio power amplifier that is able to withstand voltages up to 60 V. The audio amplifier is used in classical non-inverting and inverting voltage amplification stages. Waveforms coming from controller unit are just amplified by multiplying gain factor. It in fact added more flexibility to waveform adjustment compared to commercial solution and better results are achieved [72]. However some certain drawbacks of this design are noticed. One problem encountered is it suffers from heat dissipation at audio amplifier components. Complex design with multiple stages makes it less reliable for dynamic operations. Since the piezoelectric motor can be driven only with positive voltages the power amplifier is used in single-supply configuration. Single-supply applications

have inherent problems that dual-supply amplifier circuits often overcome. The fundamental problem is that power amplifier is a dual-supply device by itself, so biasing using external components to center the amplifiers output voltage at mid-supply is problematic. Also, operation in bending mode requires equal DC voltages to be applied to both piezo stacks (bimorph). Coupling capacitors placed at the input of the amplifier stages do not allow DC voltages to be applied thus operation only in stepping mode can be considered. Bulkiness and cost of the current design are other disadvantages. In order to overcome the mentioned design drawbacks an alternative solution is considered for this application such as switching converter. Switching converters are popular because of their flexibility in voltage levels with simply adjusting switching duty, ease of control and high efficiency. Due to the switching nature of these drivers the power losses can be reduced and heat dissipation can be overcome. The maximum rated voltage of converters are the maximum rated voltage of the MOSFETs available on the market (up to 300V). Due to the availability of integrated solutions the bulkiness and cost of the driver design can be reduced as well. The designed half bridge switching converter driver schematic is provided in Fig. 4.48. This topology basically converts input DC voltage u_i to desired voltage waveform u_o by switching on or off the transistors according to PWM duty cycle. By modulating the duty cycles desired waveforms can be acquired by the following relation

$$u_o = Du_i \quad (4.37)$$

In practical applications for this particular actuator u_i is set to 46 V DC and u_o is varied between 0 - 46 V by adjusting duty cycle D . For instance, sinusoidal duties result in sinusoidal outputs. Thus the converter provides flexibility in control of the phase voltages applied to the motor by controlling only the PWM duty cycle values.

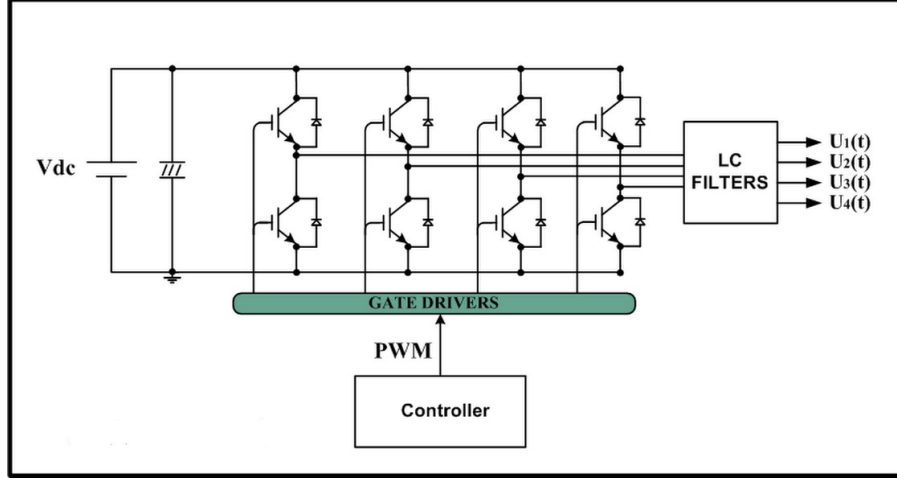


Figure 4.48: Half bridge converter schematic

4.6.2.4 Experimental results

In order to practically assess the controller for positioning an experimental setup consisting of a linear stage with motion in vertical direction is designed as shown in Fig. 4.49. Optical incremental encoder of $\mp 5nm$ pulse resolution is embedded into the stage to measure the stage displacement. Roller cage linear slides are used to provide linear low friction motion in the stage. dSPACE 1103 is employed as a controller unit with control loop of 16 KHz. Duty cycles D_1 - D_4 are the proposed controller outcomes that proportionally adjust output voltages u_1 - u_4 .

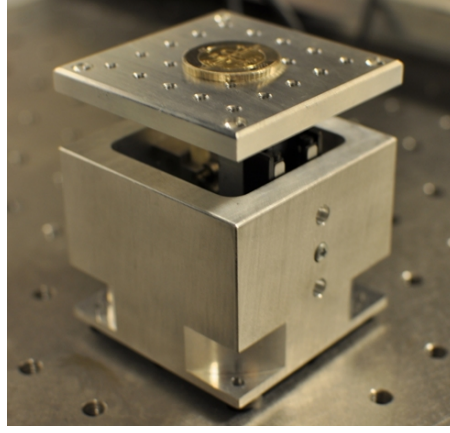


Figure 4.49: Single dimensional piezo motion stage

Step response for step reference of $100\mu m$ is given in Fig. 4.50 and zoomed view in Fig. 4.53. The controller shows excellent performance achieving fast settling time in less than $0.1s$ and residual steady state error of $75nm$. The absolute error limit to switch between macro- and micro-stepping modes has been set to $10\mu m$. The effect of the amplitude and phase modulation can be seen in the region near steady state value lasting about $0.05s$ (between $9.3s$ and $9.35s$). In the region of macro-stepping mode the actuator is driven with predefined maximum velocity, while in micro-stepping the velocity drops down due to the smaller step size and settling in this mode requires longer time. The slope of the rise/fall is dictated directly by the limit frequency. Frequency used for all experiments is $1.5KHz$.

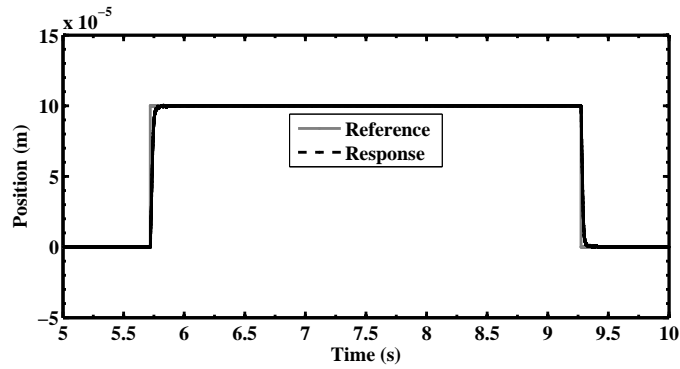


Figure 4.50: $100\mu m$ step reference response

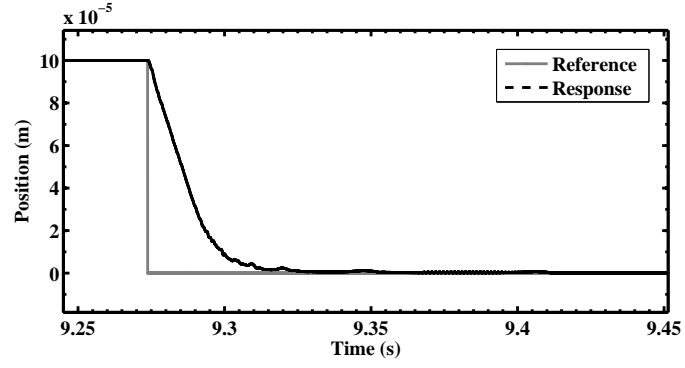


Figure 4.51: 100 μm step reference response, zoomed

For 500 μm staircase position reference a bidirectional repeatability of controller controller is tested. Staircase response is shown in the Fig. 4.52. According to the obtained results both repeatability and accuracy of the controller response is less than 75nm. Zoomed view given in Fig. 4.53. The effect of the phase and amplitude modulation can be seen between 7.14s and 7.19s.

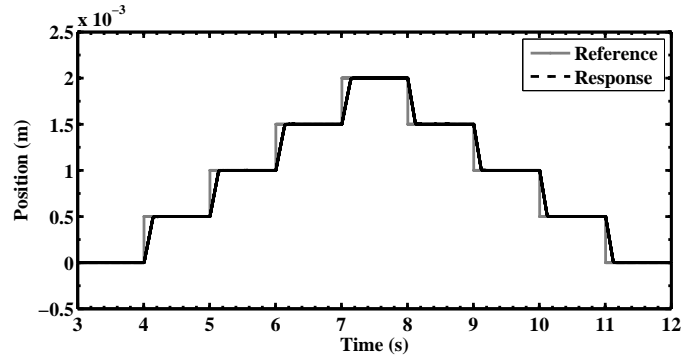


Figure 4.52: 500 μm stair case reference response

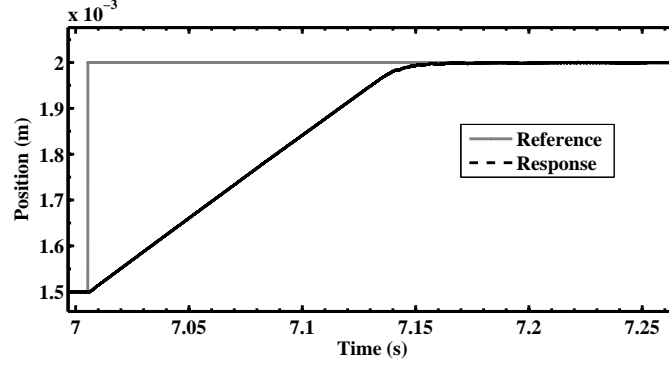


Figure 4.53: 500 μ m stair case reference response, zoomed

4.6.3 Operation in continuous mode

The highest precision down to nanometers can be achieved by operating the motor in continuous mode. As mentioned before for a single bimorph leg application of equal positive voltages results in elongation of the leg till it reaches contact with the rod thus resulting in normal force. Then by varying the amplitudes of two voltages in certain range the legs bend producing tangential force that pushes the rod in linear fashion forward or backward. Hence, by controlling the sum or difference between the applied voltages position of the legs can be adjusted [75].

4.6.3.1 Dynamical model of the legs

The dynamical model of the piezo legs in x and y dimensions can be approximated by simple mass spring damper system (MSD) [76]. In continuous mode all four legs are in clamping contact with the drive rod therefore all forces exerted by four legs should be considered. Actuator dynamical model in y coordinate is given in Fig. 4.54.

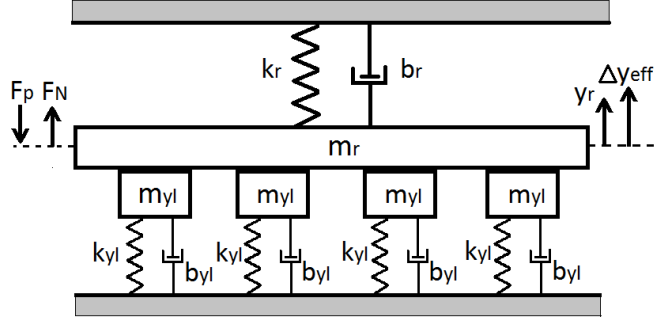


Figure 4.54: Legs and rod MSD model in y coordinate

Here, m_r is a mass of the rod, K_r is a stiffness of the ceramic material it is made of and B_r is a damping constant of the rod. m_{yl} is a mass of a single leg, k_{yl} is a stiffness of piezoceramic material and b_{yl} is a damping coefficient of the legs due to rollers, F_p is a spring preload force and F_N is a normal force exerted by the legs on drive rod. In this model surface interactions between legs and the rod are neglected hence stiction forces are considered. Mass of the rod and piezo legs are assumed to be combined. From the MSD model it can be derived that

$$M = m_r + 4m_{yl} \quad (4.38)$$

$$K = k_{yr} + 4k_{yl} \quad (4.39)$$

$$B = b_{yr} + 4b_{yl} \quad (4.40)$$

then the normal force can be expressed as follows

$$F_N = < F_{ipe} - F_p > \quad (4.41)$$

where F_p is a force applied by the spring pre-load and F_{ipe} is a total force due to inverse piezoelectric effect of four legs which is a sum of forces applied by each leg. According to Eq. 4.41 in order to produce motion in x plane the normal force F_N

should be greater than zero above some threshold thus F_{ipe} should be always greater than F_p . Then the dynamical equation for motion in y plane can be finalized as

$$M\ddot{y}_r + B\dot{y}_r + Ky_r = F_N \quad (4.42)$$

Legs dynamics in x direction can be described as interaction between legs and the rod as depicted in Fig. 4.55. In this model since piezo legs and the drive rod are in clamping contact, no relative motion between the legs and the rod exists. Hence, kinetic friction forces are not considered and only static friction force f_s is taken into account which is

$$f_s \leq \mu_s F_N \quad (4.43)$$

here f_s is a stiction force, μ_s is a friction coefficient and F_N is a normal force applied by the legs on drive rod. Hence, in order to produce motion of the rod in horizontal direction with no slip, legs should exert enough normal force on the rod. Once this condition is satisfied then the overall dynamical equation of the rod and the legs combined in x dimension can be written given that

$$M = m_r + 4m_{xl} \quad (4.44)$$

$$K = 4k_{xl} \quad (4.45)$$

$$B = b_{xr} + 4b_{xl} \quad (4.46)$$

$$M\ddot{x}_r + B\dot{x}_r + Kx_r = < F_x - F_l > \quad (4.47)$$

then

$$M\ddot{x}_r + B\dot{x}_r + Kx_r = F_T \quad (4.48)$$

From the Eq. 4.47 it can be inferred that in order to generate a motion in x plane and tangential force F_T the force F_x generated by bending action of the legs should

be greater than the load force F_l that is a sum of applied external forces and forces due to rollers.

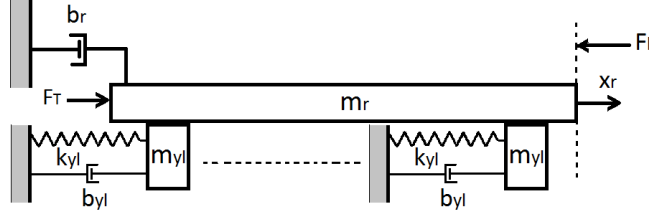


Figure 4.55: Legs and rod MSD model in x coordinate

4.6.3.2 Static model and identification

In order to verify static relations experimentally in this mode an identification experiment is conducted. From the theoretical relations given in Eq. 4.17 and Eq. 4.18 the leg motion in x direction is a result of the voltage difference applied to the bimorph and the elongation of the leg in y direction is related to the sum of the voltages. The relation between rod displacement in y plane versus sum of the applied voltages is plotted in Fig. 4.56 and motion of the rod in x plane versus voltage difference is given in Fig. 4.57. Here, all four legs are considered to perform the same motion. In Fig. 4.56, equal voltages are applied to both stacks of the bimorphs then it is gradually increased so that legs elongate pushing the rod against the spring load. For measuring displacement in this coordinate the position measurement device scale is placed in the direction of elongation. In Fig. 4.57, the voltage difference is gradually varied with certain steps and the motion of the rod is measured in x coordinate. A certain voltage is applied to all four legs in order to them to be in contact with the rod then voltages are varied and the rod motion is continuously measured. Voltages are applied in such manner that for each of four legs one stack of a bimorph is pushed up increasing voltage with certain steps when the other stack is pulled down thus voltage is lowered with the same steps resulting in overall bending. The resultant

plots demonstrate approximately linear relation between leg position in both coordinates and applied voltages as proposed in theoretical model. The slopes of the graphs are estimated as $K_1 = 7.17 \times 10^{-8}$ and $K_2 = 2.94 \times 10^{-8}$, respectively.

These plots allow us to identify the system limits in this mode. Minimum displacement of the legs in x can be given by the following relation

$$\Delta x_{min} = K_1(\Delta u_{min}) \quad (4.49)$$

here, Δu_{min} is a minimum voltage difference that generates motion in x dimension where Δu_{min} is measured at $0.055V$ and substituting K_1 into Eq. 4.49 Δx_{min} is calculated as $3.94nm$ that corresponds to a value within one encoder pulse.

The minimum displacement at which four legs are in first contact with the rod can be given as

$$\Delta y_{cont} = K_2(u_{cont}) \quad (4.50)$$

Here, Δy_{cont} and u_{cont} are the normal displacement and the minimum voltage to be applied. The minimum voltage at which the first change in position is observed is at $u_{cont} = 0.5078V$ then the Δy_{cont} is calculated substituting values into Eq. 4.50 where $\Delta y_{cont} = 0.149\mu m$.

Similarly, the maximum elongation and deflection capabilities of the legs together with the rod can be determined. The maximum displacement in horizontal direction is found to be at maximum voltage difference of $\Delta u_{max} = 43.7V$ meaning in displacement of approximately $\Delta x_{max} = 3.1\mu m$ in one direction where elongation is limited to the maximum voltage that can be applied to the system which is $u_{max} = 46V$ and it corresponds to approximately $\Delta y_{max} = 2.7\mu m$.

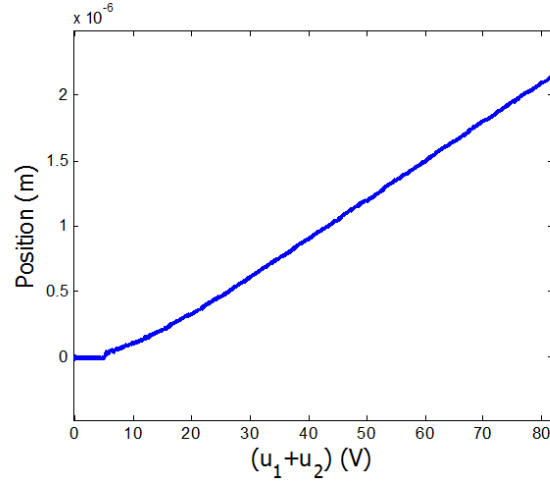


Figure 4.56: Rod displacement in y direction vs. sum of phase voltages

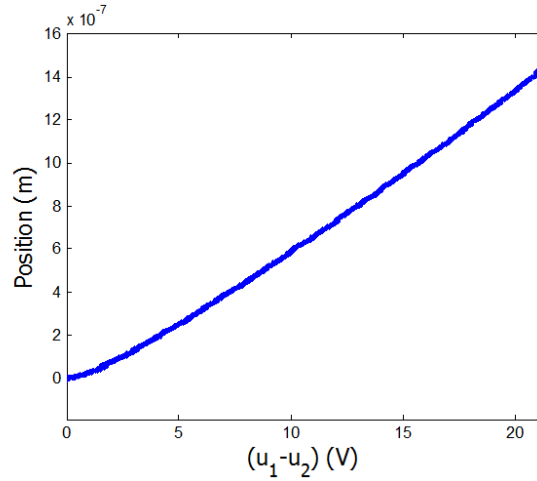


Figure 4.57: Rod displacement in x direction vs. difference of phase voltages

4.6.3.3 Dynamical model parameters identification

Dynamical model defines the system behavior for certain inputs, stability criterion and its resonance to design a proper controller. Since the effective motion in x is considered the dynamical model parameters in x direction are derived based on step response in continuous mode. For this purpose relatively large voltages difference applied to the legs and step response plot is recorded. Then a parametric time

domain system identification analysis is performed for MSD model. Since mass of the legs and rod are known then the system stiffness and damping constants can be estimated based on system response data. Damped natural frequency of the system can be expressed as

$$w_d = \frac{\pi}{t_p} \quad (4.51)$$

where π is a mathematical constant and t_p is a peak time of the response plot. Percent overshoot can be given as

$$PO = \frac{y_{peak} - y_{ss}}{y_{ss}} \quad (4.52)$$

here, y_{peak} and y_{ss} are the peak and steady state responses respectively. The the damping ratio of the system is

$$\zeta = \sqrt{\frac{(\ln PO)^2}{(\ln PO)^2 - \pi^2}} \quad (4.53)$$

The stiffness of the system can be determined from the equation

$$w_d = \sqrt{\frac{K}{M}} \sqrt{1 - \zeta^2} \quad (4.54)$$

Since the combined mass of the legs and the rod is known, by substituting the calculated parameters stiffness K can be derived. Similarly the damping constant can be calculated from

$$B = \frac{2\zeta K}{w_d} \sqrt{1 - \zeta^2} \quad (4.55)$$

The second order transfer function of the system can be expressed as

$$T(s) = \frac{X(s)}{F_T(s)} = \frac{\alpha}{Ms^2 + Bs + K} \quad (4.56)$$

where α is a scaling constant relating deflection and force. Assuming the linear relation between applied voltage and the force exist then the equation can be rewritten as

$$T(s) = \frac{X(s)}{U(s)} = \frac{\beta}{Ms^2 + Bs + K} \quad (4.57)$$

where β is a scaling constant relating voltage to deflection. The actual step response plot and the estimated model response plot for the same voltage difference input is depicted in Fig. 4.58.

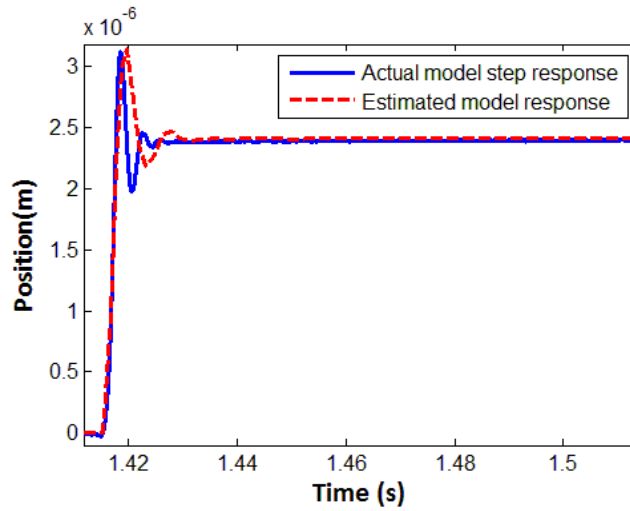


Figure 4.58: Actual and estimated system step response plots

4.6.3.4 Controller scheme

Based on identification experiments the model is assumed to be linear and a PI controller is proposed to achieve desired positioning. By controlling the difference

between the applied voltages a position control in x dimension can be achieved. The proposed controller scheme is designed as follows

$$e_p = x^{ref} - x^{meas} \quad (4.58)$$

$$u = K_p e_p + K_i \int e_p dt \quad (4.59)$$

$$\begin{pmatrix} u_1 \\ u_2 \end{pmatrix} = \frac{1}{2} \underbrace{\begin{pmatrix} 1 & 1 \\ -1 & 1 \end{pmatrix}}_{H_2} \begin{pmatrix} u \\ u_N \end{pmatrix} \quad (4.60)$$

$$x^{des} = K(u_1 - u_2) \quad (4.61)$$

From the controller equations above x^{ref} and x^{meas} are the reference and measured positions respectively, and e_p is error in position. u is a control voltage which is a result of PI controller that pushes e_p to zero also minimizing the steady state error. Since the system requires two inputs u_1 and u_2 the calculated u control action is further decoupled by Hadamard transformation H_2 of u and u_N vector in Eq. 4.60. A Hadamard matrix is useful for the transformation of variables into common and differential modes, which relates to the functions. In other words, this coordinate transformation performs modal decomposition. It also satisfies the both conditions given in Eq. 4.17- 4.18 thus the sum of the voltages is equal to a certain voltage u_N at which the legs produce enough normal force to result in stiction of the legs to the rod. This enables further bending of the legs to be able to push the drive rod in x plane with no slip when the difference in voltage is u that is a controller output. Hence, calculated control output sets the position of the motor in desired position in x coordinate.

4.6.3.5 Experimental results

In order to assess the controller for positioning in bending mode the same experimental setup consisting of a linear stage with motion in vertical direction is used. dSPACE 1103 is used as a controller unit and the designed half bridge switching converter driver [73] is employed to drive the motor. Duty cycles d_1 and d_2 are the controller outcomes. Only DC voltages are considered to drive the legs in bending mode.

Experimental results for staircase response of the actuator with 50 and 10 nm steps are provided in Fig. 4.59 and Fig. 4.61, respectively.

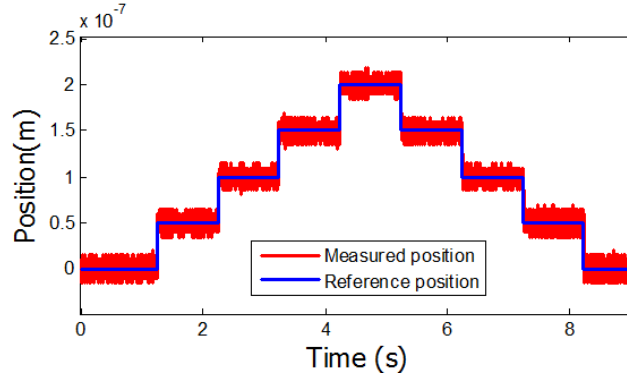


Figure 4.59: 50 nm stair case response

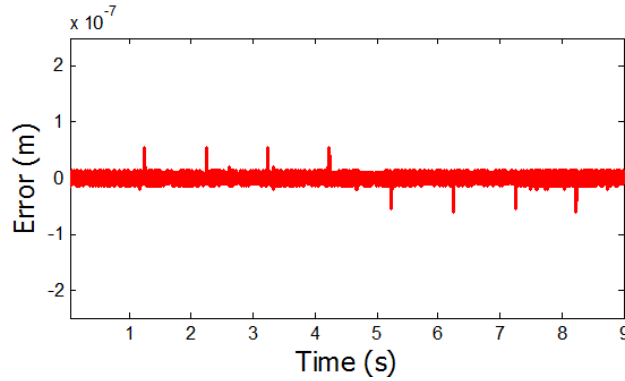


Figure 4.60: 50 nm stair case error

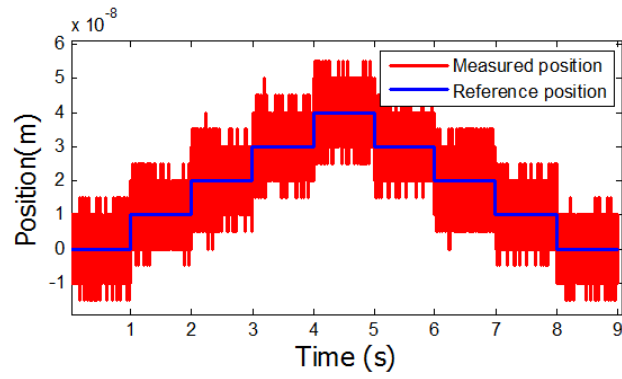


Figure 4.61: 10 nm stair case response

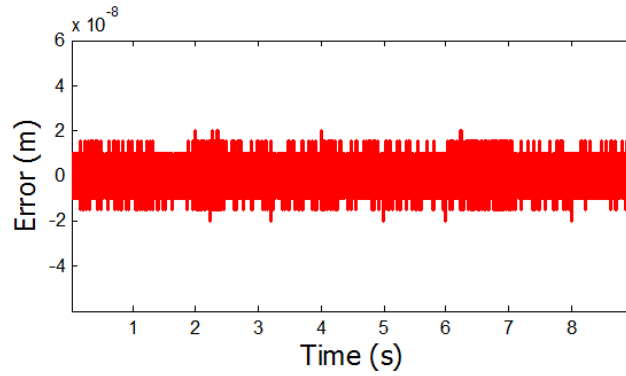


Figure 4.62: 10 nm stair case error

Sinusoidal reference tracking of 100 nm peak to peak amplitude and frequency of 1 Hz is given in Fig. 4.63.

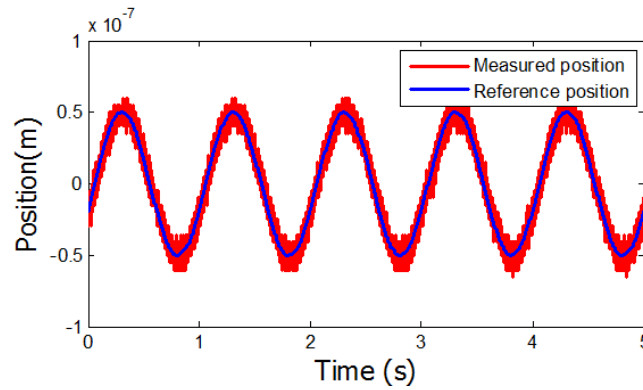


Figure 4.63: 100 nm p-p sinusoidal reference tracking response

From the Fig. 4.62 it can be seen that error in positioning is $\pm 5nm$ with some jumps in measurement device. Taking the fact that commercial encoder has nominally dithering pulses of $\pm 5nm$ due to electronics, the error can be interpreted to be due to measurement noise related to environmental disturbance. This behavior can be observed primarily when no control action is applied to the system and can not be avoided without employment of special isolation equipment. Despite this fact, overall performance of the controller demonstrate accurate positioning response of the system for very small displacements.

4.6.4 High precision positioning stage design

High precision positioning stages are widely employed to precisely deliver a specimen to a desired destination. They are also useful for scanning and micromachining of the micro systems. Since precise control and drive of the piezoelectric motor is achieved a design of two DOF of positioning stage is proposed for fine positioning of the micro parts within the microfactory concept. The conceptual and manufactured designs are presented in Fig. 4.64 and Fig. 4.65, respectively.

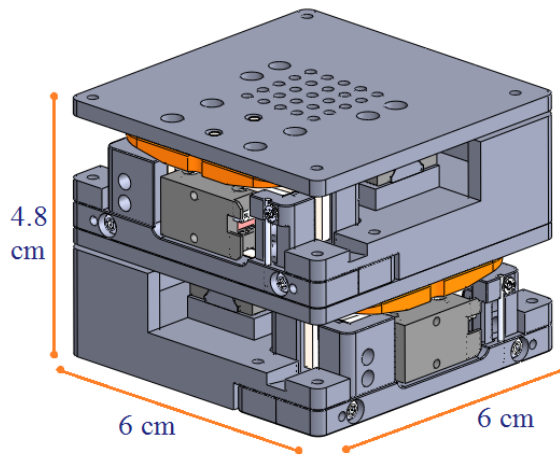


Figure 4.64: Two dimensional high precision positioning stage CAD drawing

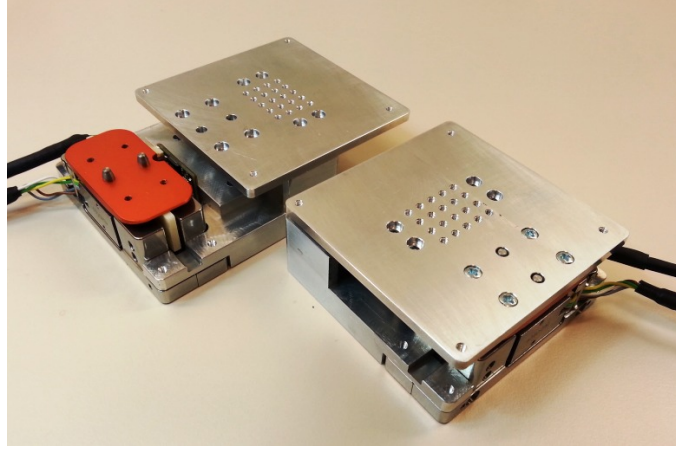


Figure 4.65: Manufactured and assembled high precision positioning stage

The stage is compact in size having dimensions of $6\text{cm} \times 6\text{cm} \times 4.8\text{cm}$ and can be easily incorporated into the system. Two PiezoLEGS Caliper motors are used to precisely drive the stages in x-y plane. Piezowalkers utilized here slightly differs from those of discussed previously just from structural point of view. These actuators have two sets of walking legs residing within the motor housing thus 4 legs at both sides of the rod totally of 8 legs are embedded in order to double driving and stall force characteristics (refer to Fig. 4.66). In other words, it can be assumed that two motors are merged together to drive the rod and result in more powerful actuation. The Piezo LEGS Caliper is designed for stage integration. It is miniaturized to a degree where it will fit inside a linear stage or a goniometer stage. The motor is easily mounted in the stage blocks using eight screws.

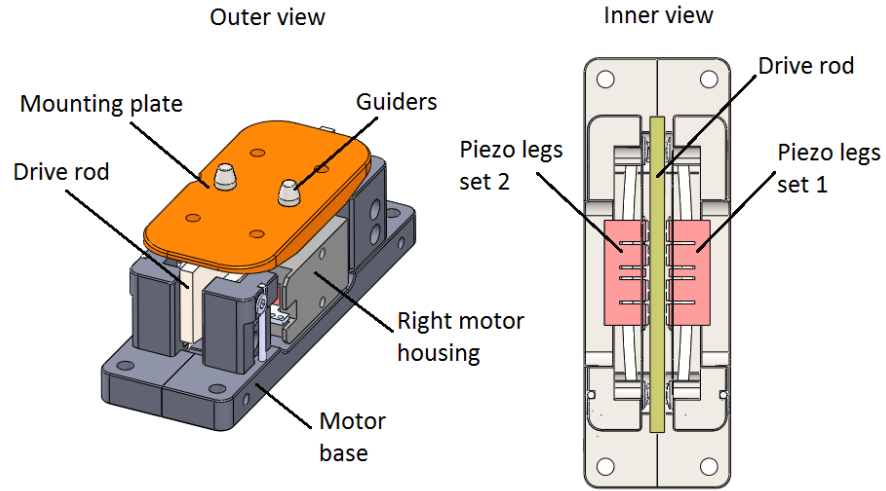


Figure 4.66: Piezo calliper motor scheme

According to the vendor's specifications such structure is capable of driving loads up to 20 N. It makes it more effective and reliable for positioning with high accuracy of much higher loads compared to stage weight and size. Since the operational principle of the "8-legged" motor remains the same with that of "4-legged", control and driving techniques are valid for both types. The proposed motion stage can be utilized for any two dimensional high precision positioning applications. Within the scope of microfactory project it is considered to be further employed under galvanometric laser scanning system to increase working area and complexity of machining by synchronizing together with galvo mirrors.

4.7 Software Design

4.7.1 Software Organization

Once all of the modules are ready they are assembled together to a microfactory concept for further cooperative tasks. As mentioned before each unit is self-sufficient with its control software. However operation in cooperative way requires organization

of overall software in order to set a certain decision logic and communication between the modules. It is also useful to keep parallelism in processing with no overheads and latency. Therefore each software code running behind the functional units is partitioned into five functions running inside two real time loops. The reason of such approach is due the capabilities of the dSPACE controller platform to run two real time loops at once. Keeping each chunk of code pertaining to a specific module as a function would keep the modularity and simplicity of organizing the overall system. Decision when to run the modules is done based on state machine logic. Idea behind the state logic here is to operate all four processing units upon rotary conveyor system state. If the rotational transportation system is delivered and stationed a specimen to the modules it rises a ready flag after which units start to process the sample in question. Similarly, when the tasks are accomplished by all modules (with the last module finishing its task) the ready flag is raised again and the delivery system proceeds to next rotation task.

For testing the complete system a simple application is considered in the beginning. The system is set as in Fig.4.67 and the process flow is considered as shown in Fig.4.68.

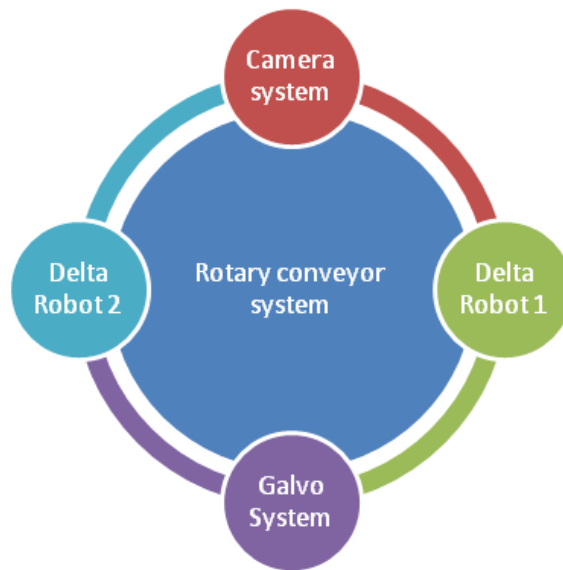


Figure 4.67: Possible system organization

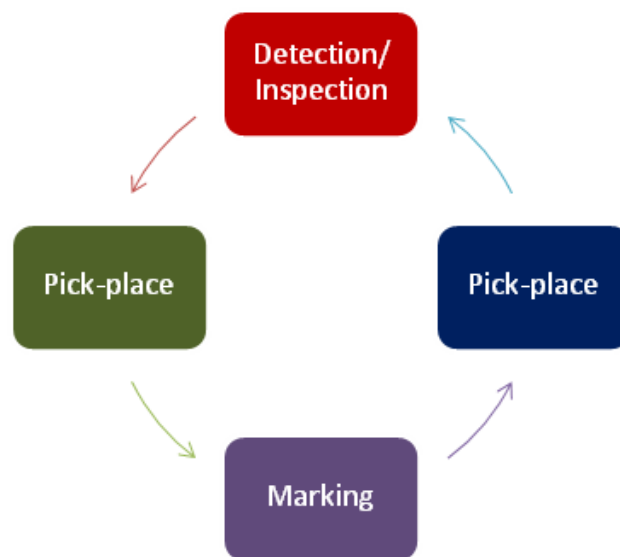


Figure 4.68: Possible process flow

Let's consider a simple process with marking of a certain pattern on a tiny metallic ball. Then a sample plate should have holes in order balls sit on them. Plate can be segmented into five areas as depicted in Fig.4.69; detection area where balls are going to reside initially and camera determines their current positions, machining area at

the center of the plate for galvo system to mark a certain image on it, inspection area where machined balls are examined for correctness of the pattern, two more segments at the bottom where proper and faulty parts reside after decision of the inspection unit.

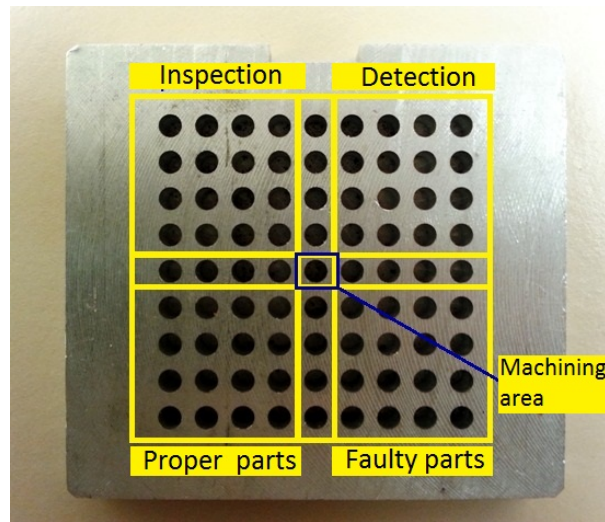


Figure 4.69: Sample plate organization

For this particular example, the process flow can be organized as follows; once a ball specimen is positioned into "Detection area" of sample plate the rotary conveyor system primarily proceeds to a homing procedure, then the specimen is delivered to initial processing module which in this case is the camera system. Entire sample plate needs to be scanned and specimens are detected in the beginning in order to identify their positions on sample plate. Current position information is provided to the function running behind the next module in question as a reference for further tasks. Therefore, since pick-place is a second task to be performed on this specimen the position information received from the camera function is passed to the delta robot function. When conveyor mechanism delivers the specimen to delta robot, it will already contain data where exactly the specimen is located. It picks the sample and places it into the machining area at the center of the sample plate. Rotation is

performed once more for galvo system to further machine or mark a certain pattern on a ball specimen. Then the conveyor system runs forward to the second delta robot for it to pick and place the part into the "Inspection area". This is done in order for camera system finally inspect and check the validity of the machined image. If the pattern is accepted to be satisfactory then the system proceeds to the next delta robot for placing the micro part to a "Proper parts" area. In other case it places it to a "Faulty parts" section. By such approach operator may keep track of successful and faulty parts that are machined by just looking at the segmented area on the plate. Short example of program flow for this particular application can be described by pseudocodes as follows

```

-----
conveyorHoming();
if conveyorHoming == Done then
    cameraDetection();
else
    cameraWait();
end if
if cameraDetection == Done then
    conveyorRotation();
else
    conveyorWait();
end if
if conveyorRotation == Done then
    deltaPickPlace(samplePos);
else

```

```
    deltaWait();
```

```
end if
```

```
-----
```

Similarly, for inspection and separation of the machined parts into correct and faulty categories can be done as given bellow:

```
-----
```

```
cameraInspection();
```

```
if cameraInspection == Done then
```

```
    conveyorRotation();
```

```
    if conveyorRotation == Done then
```

```
        if sampleImage == Proper then
```

```
            deltaPickPlace(properRefPos);
```

```
        else
```

```
            deltaPickPlace(faultyRefPos);
```

```
        end if
```

```
    else
```

```
        deltaWait();
```

```
    end if
```

```
else
```

```
    conveyorWait();
```

```
end if
```

```
-----
```

4.7.2 Human Machine Interface

For ease of interaction between the system and the operator a need for a Human Machine Interface (HMI) arises. The role of HMI is to allow users simply control the system by setting desired references and also observe system operational flow at any instant of time. By that way user can operate the system through graphical interface so he or she doesn't have to burden him/herself with the details of the codes running behind the system.

4.7.2.1 GUI

Designed Graphical User Interface (GUI) for microfactory under consideration in this work is demonstrated in Fig.4.70 and Fig.4.71, respectively. It consists of file menu at the top of the display, tabs for transition between control panels of the modules and red/green indicator lamps for module activities at the bottom of the GUI. Moreover there is an emergency stop bottom for safety purposes. This GUI allows users to set, observe and control each module separately through single display.

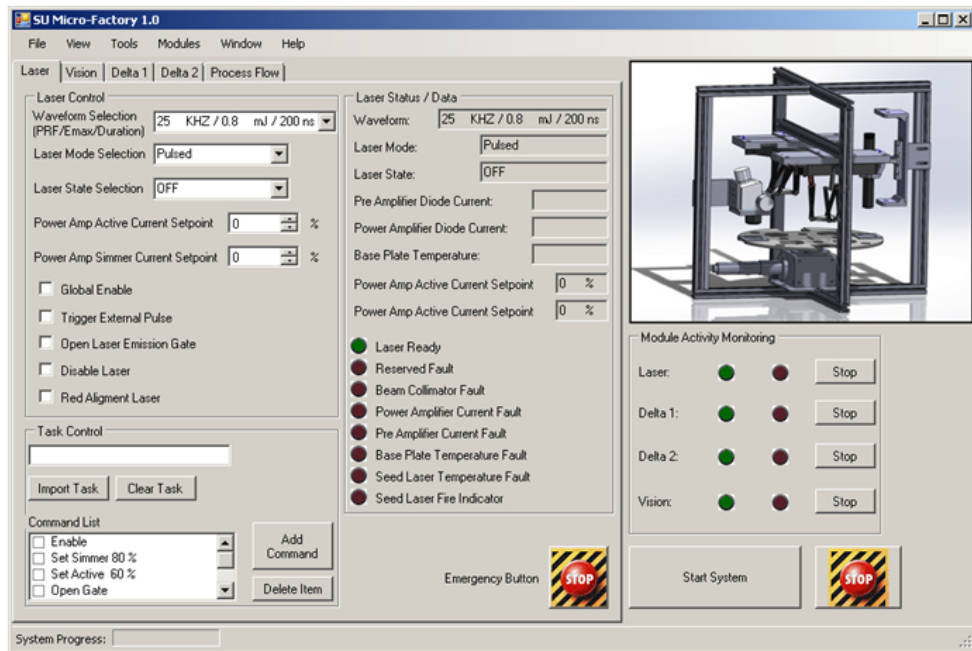


Figure 4.70: Microfactory GUI, Laser control panel

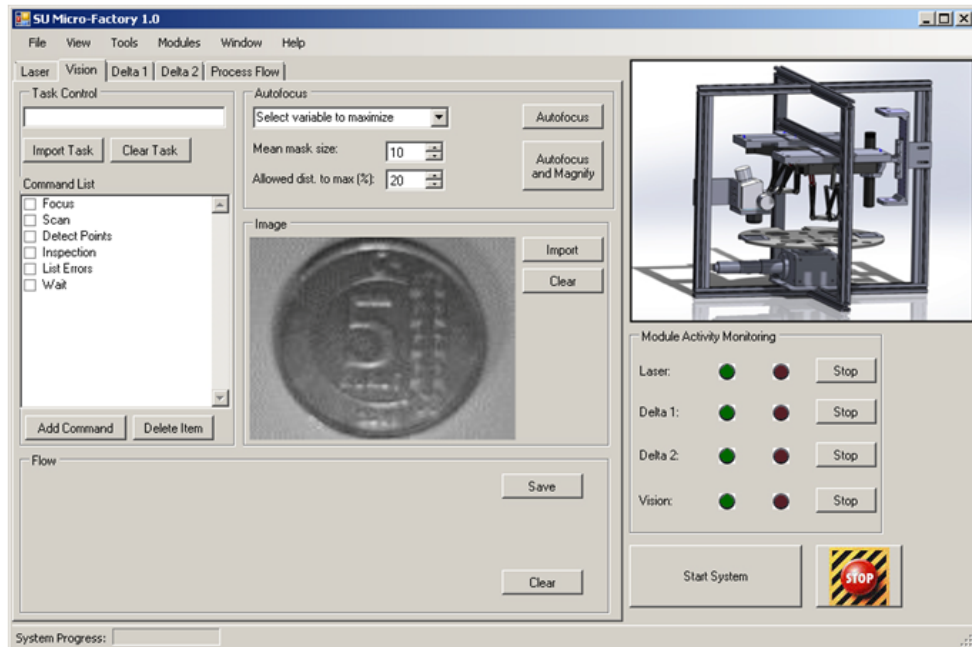


Figure 4.71: Microfactory GUI, Vision control panel

4.7.2.2 Software/Hardware interface

The purpose of interface electronics is to set connection between supervision computer and hardware residing in the system. Control commands coming from software program are provided to the modules through electronic connector boards as shown in Fig.4.72 below. Whole structure consist of a main board that connects user PC to the rest of the microfactory sub systems and small boards for each module. Such structure enables modular operation meaning that modules can be disconnected from the whole system and operate alone.

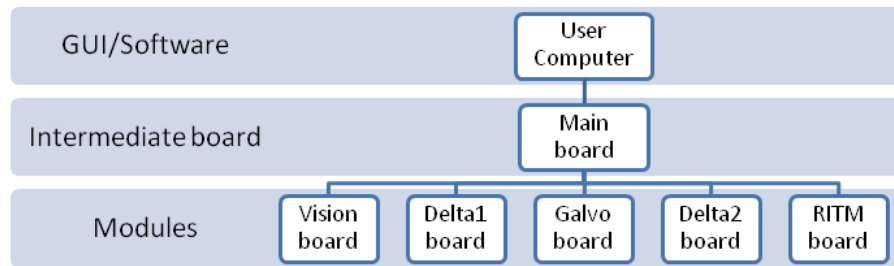


Figure 4.72: Software to hardware interface structure

Schematics of some electronic connector boards are provided in Fig.4.73. Circuits are designed on Eagle software program and sent for manufacturing. Main board consists of multi pin connectors where necessary power supply, analog, digital and encoder interfaces of the dSPACE computer are attached. Each module board consist of one main connector to set connection with the main board and particular I/O interfaces needed for operating the modules.

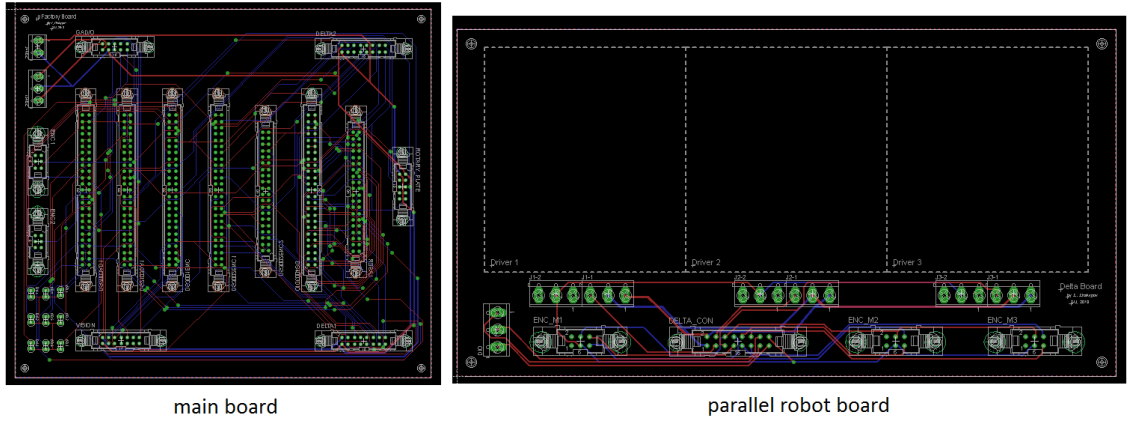


Figure 4.73: Main and delta robot board schematics

Once interface boards are produced and assembled then a complete operation of the microfactory can be expected. Therefore experimental results for complete microfactory system are not provided and it is left beyond the scope of this thesis work.

5 CONCLUSION AND FUTURE WORK

This work presented the design steps and implementation of a modular and reconfigurable desktop microfactory for high precision machining and assembly applications as a proof of concept. Proposed system is constructed based on some functional, performance and design criteria such as miniature size, modularity, reconfigurability, accuracy in sub-millimeters, ease of transportation and integration. It consists of downsized functional modules such as two parallel kinematic robots for manipulation and assembly, galvanometric laser beam scanning system for 2D micromachining, high precision piezoelectric positioning stage, camera system for detection and inspection, and a rotational conveyor system. Design of the modules comprises development of mechanical structure, electronic driver and communication interface, and control approach for each unit. Each module is designed and tested for fine precision applications in the beginning. Once stand-alone operation of each unit is achieved further assembly to a single microfactory system has been considered. The mechanical structure of the miniature factory is constructed in such manner that it allows parallel processing, flexible rearrangement of the layout, and ease of assembling and disassembling of the units and overall design as general.

Several paper works are presented or in press to be published in various international conferences and proceedings in contribution to the literature within the scope of the thesis. Main contributions are related to

- Mathematical modeling and fine control of a galvanometric laser beam steering system with few micron precision marking capabilities;

- Modeling, design and control of high precision positioning stage built on walking piezoelectric motors with micro and nanometer positioning accuracy;
- Design and control of an intermodular transportation mechanism for sample delivery;
- Design of flexible and reconfigurable mechanical structure of the desktop microfactory system;
- Design of electronic interface for each module;
- Development of software organization and GUI.

Further works are considered to be addressed to setting experiments with the overall system, possible implementation of the system for simple tasks and integration of different techniques and modules for more complex processes. Development of a second version of the desktop microfactory based on the current knowledge can be also considered as a possible future work.

Bibliography

1. Okazaki, Y.; Mishima, N.; Ashida, K.; , "Microfactory and Micro Machine Tools," The 1st Korea-Japan Conference on Positioning Technology, Daejeon, Korea, 2002.
2. Okazaki, Y., Mishima, N., and Ashida, K. (2004). Microfactory Concept, History, and Developments. *Journal of Manufacturing Science and Engineering*, 126(4), 837.
3. Kawahara, N., Suto, T., Hirano, T., Ishikawa, Y., Kitahara, T., Ooyama, N., Ataka, T. (1997); Microfactories; new applications of micromachine technology to the manufacture of small products. *Journal of Microsystem Technologies*, Springer-Verlag, pp. 37-41, 1997.
4. T. Ataka, "The Experimental Microfactory System in Japanese national *R&D* Project," Singapore-Japan Forum on MEMS, 23 November 2000, Singapore.
5. Qin, Y., Brockett, a., Ma, Y., Razali, a., Zhao, J., Harrison, C., Pan, W., Dai, X., Loziak, D. (2009). Micro manufacturing: research, technology outcomes and development issues. *The International Journal of Advanced Manufacturing Technology*, 47(9-12), 821837.
6. Kussul E., Ruiz L., Caballero A., Kasatkina l., Baydyk T; CNC machine tools for low cost micro devices manufacturing; First International Conference on Mechatronics and Robotics; St.- Petesburg, Russia; 2000, Volume1; pp 98-103.
7. Ito, S.; Iijima, D.; Hayashi, A.; Aoyama, H.; Yamanaka, M.; "Micro turning system: A Super Small CNC Precision Lathe for Microfactories," *Proceedings of the 3rd International Workshop on Microfactories*, pp. 3740, 2002.

8. Probst, M.; Vollmers, K.; Kratochvil, B. E.; Nelson, B. J.; , "Design of an Advanced Microassembly System for the Automated Assembly of Bio-Microrobots," in Proceedings of 5th International Workshop on Microfactories, 2004.
9. Dechev, N.; Lu Ren; Liu, W.; Cleghorn, L.; Mills, J.K.; , "Development of a 6degree of freedom robotic micromanipulator for use in 3D MEMS microassembly," Robotics and Automation, 2006. ICRA 2006. Proceedings 2006 IEEE International Conference on , vol., no., pp.281-288, 15-19 May 2006.
10. Xinhan Huang; Xiadong Lv; Min Wang; , "Development of A Robotic Microassembly System with Multi-Manipulator Cooperation," Mechatronics and Automation, Proceedings of the 2006 IEEE International Conference on , vol., no., pp.1197-1201, 25-28 June 2006.
11. Burisch, A., Wrege, J., Raatz, A., Hesselbach, J., & Degen, R. (2007). PARVUS miniaturised robot for improved flexibility in micro production. *Assembly Automation*, 27(1), 6573.
12. Kunt, E.D.; Naskali, A.T.; Sabanovic, A., "Miniaturized modular manipulator design for high precision assembly and manipulation tasks," *Advanced Motion Control (AMC)*, 2012 12th IEEE International Workshop on , vol., no., pp.1,6, 25-27 March 2012.
13. Kunt, E.D.; Naskali, A.T.; Cakir, K.; Sabanovic, A.; Yuksel, E.; , "A Versatile and Reconfigurable Microassembly Workstation," *Proceedings of the International Workshop on Microfactories*, 2008. IWMF08, pp. 37-41, October 2008.
14. Heikkila, R.H.; Karjalainen, I.T.; Uusitalo, J.J.; Vuola, A.S.; Tuokko, R.O.; , "Possibilities of a Microfactory in the Assembly of Small Parts and Products

- First Results of the M4-project,” Assembly and Manufacturing, 2007. ISAM '07. IEEE International Symposium on, vol., no., pp.166-171, 22-25 July 2007.
15. Fatikow, S.; Seyfried, J.; Fahlbusch, S.; Buerkle, A.; Schmoeckel, F., ”A flexible microrobot-based microassembly station,” Emerging Technologies and Factory Automation, 1999. Proceedings. ETFA '99. 1999 7th IEEE International Conference on, vol.1, no., pp.397-406 vol.1, 1999.
 16. Woern, H.; Seyfried, J.; St. Fahlbusch; Buerkle, A.; Schmoeckel, F., ”Flexible microrobots for micro assembly tasks,” Micromechatronics and Human Science, 2000. MHS 2000. Proceedings of 2000 International Symposium on , vol., no., pp.135-143, 2000.
 17. Aoyama, H.; Iwata, Futoshi; Sasaki, Akira, ”Desktop flexible manufacturing system by movable miniature robots-miniature robots with micro tool and sensor,” Robotics and Automation, 1995. Proceedings., 1995 IEEE International Conference on , vol.1, no., pp.660,665 vol.1, 21-27 May 1995.
 18. Verettas, I.; Clavel, R.; Codourey, A., ”PocketFactory : a modular and miniature assembly chain including a clean environment,” Proceedings of the 6th International Workshop on MicroFactories IWMF 2006, October 2006.
 19. E. Kussul, T. Baidyk, L. Ruiz-Huerta, A. Caballero-Ruiz, G. Velasco, and L. Kasatkina, ”Development of micromachine tool prototypes for microfactories,” Journal of Micromechanics and Microengineering, vol. 12, no. 6, pp. 795812, 2002.
 20. Vogler, M.P.; Liu, X.; Kapoor, S.G.; Devor, R.E., ”Development of Mesoscale Machine Tool (mMt) Systems”, Transactions of the North American Manufacturing Research Institution of SME, pp. 653-652, 2002.

21. Dornfeld, D., Min, S., & Takeuchi, Y. (2006). Recent Advances in Mechanical Micromachining. *CIRP Annals - Manufacturing Technology*, 55(2), 745-768.
22. Ivano Beltrami, Cdric Joseph, Reymond Clavel, Jean-Philippe Bacher, Stefano Bottinelli, Micro- and nanoelectric-discharge machining, *Journal of Materials Processing Technology*, Volume 149, Issues 13, 10 June 2004, Pages 263-265.
23. Suda, M.; Furata, K.; Sakuhara, T.; Akata, T.; "The microfactory system using electrochemical machining", *Galvanotechnik Journal*, Japan, 2000, vol. 90, No 9, p. 2607-2609.
24. Gnian Cher Lim ; Tuan-Anh Mai; Laser microfabrication: present to future applications. *Proc. SPIE 4426*, Second International Symposium on Laser Precision Microfabrication, 170, February 19, 2002.
25. Prusi T, Uusitalo J, Heikkil R, Tuokko R (2008), Visual on-line measurement in a laser micro lathe. *Proceedings of the 6th International Workshop on Microfactories IWMF 2008*, October 2008.
26. Seung-Kook Ro; Sung-Kweon Jang; Byung-Sub Kim; Jong-Kweon Park, "Development of a Miniature Vertical Milling Machine for Automation Used in a Microfactory," *Smart Manufacturing Application*, 2008. *ICSMA 2008*. International Conference on , vol., no., pp.186,189, 9-11 April 2008.
27. Sung-Hyun Jang; Yong-Min Jung; Hyun-Young Hwang; Young-Hyu Choi; Jong-Kwon Park, "Development of a Reconfigurable Micro Machine Tool for Microfactory," *Smart Manufacturing Application*, 2008. *ICSMA 2008*. International Conference on , vol., no., pp.190,195, 9-11 April 2008.
28. Qin, Y. (2006). Micro-forming and miniature manufacturing systems development needs and perspectives. *Journal of Materials Processing Technology*,

177(1-3), 818.

29. Naskali, a. T., Kunt, E. D., & Sabanovic, a. (2012). Bi-level modularity concept within a robotic assembly module of a microfactory setting. *The International Journal of Advanced Manufacturing Technology*, 66(9-12), 12551269.
30. Gaugel, T.; Dobler, H., Nelson, B.J.; , "Advanced Modular Micro-Production System (AMMS)," *Proceedings of SPIE The International Society for Optical Engineering* 4568, 2001, pp. 278-285.
31. Gaugel T.; Dobler H.; Rohrmoser B.; Klenk J.; Neugebauer J.; Schfer W.; (2000) Advanced modular production concept for miniaturized production. 2nd International Workshop on Microfactories. IWMF 2000:3538.
32. Kunt, E.D., "Microfactory Concept with Bilevele Modularity", PhD Thesis, 2011, Sabanci University, Istanbul, Turkey.
33. Eray A. Baran, Orhan Ayit, Victor B. Santiago, Sergio L. D. Guerra and Asif Sabanovic; "A Self Optimizing Autofocusing Scheme for Microscope Integrated Visual Inspection Systems", (ECC13) 12th biannual European Control Conference, Zurich, Switzerland (In press).
34. Meijer, Johan, Laser beam machining (LBM), state of the art and new opportunities, *Journal of Materials Processing Technology*, 149 (1-3). pp. 2-17 2004.
35. Nadeem H Rizvi, Paul Apte, Developments in laser micro-machining techniques, *Journal of Materials Processing Technology*, Volume 127, Issue 2, 30 September 2002, Pages 206-210.
36. Rensch, Clemens; Hell, Stefan; von Schickfus, Manfred; Hunklinger, Siegfried,

- Laser scanner for direct writing lithography, *Applied Optics*, Volume 28, Issue 17, September 1, 1989, pp.3754-3758.
37. Xie Zexiao, Wang Jianguo, Jin Ming, Study on a full field of view laser scanning system, *International Journal of Machine Tools and Manufacture*, Volume 47, Issue 1, January 2007, Pages 33-43.
 38. H.J. Booth, Recent applications of pulsed lasers in advanced materials processing, *Thin Solid Films*, Volumes 453/454, 1 April 2004, Pages 450-457.
 39. Podoleanu A. G., Rogers J. A., Jackson D. A., Dunne S., "Three dimensional OCT images from retina and skin," *Opt. Express* 7(9), 2922-2938 (2000).
 40. Ming-Fei Chen, Yu-Pin Chen, Wen-Tse Hsiao, Shi-Yuan Wu, Chun-Wei Hu, Zhi-Peng Gu, A scribing laser marking system using DSP controller, *Optics and Lasers in Engineering*, Volume 46, Issue 5, May 2008, Pages 410-418.
 41. F. Blais, "Control of low inertia galvanometers for high precision laser scanning systems," *Opt. Eng.* 27(2), 104-110 (1988).
 42. Chen, Ming-Fei; Ho, Yu-Sen; Chung, Chien-Kai; Huang, Wei-Lun; Wang, Shen-Mao, Examination of the Developed Scanning System for RedGreenBlue Laser Projector with a Feedback Control, *Optical Review*, Volume 18, Issue 1, pp.128-131., January 2011.
 43. Jing Feng; Jiang Zhi, "Digital implementation of a galvanometric optical scanner based on DSP and FPGA," *Mechatronic Science, Electric Engineering and Computer (MEC)*, 2011 International Conference on , vol., no., pp.1899-1902, 19-22 Aug. 2011.
 44. http://www.thorlabs.com/NewGroupPage9.cfm?objectgroup_id=6057, Large Beam Diameter Scanning Galvo System, last view July, 2013.

45. Zhenishbek Zhakypov, Edin Golubovic, Asif Sabanovic, Galvanometric Optical Laser Beam Steering System for Microfactory Application, (IEEE IES) IEO-CON13 - 39th Annual Conference of the Industrial Electronics Society, Vienna, Austria, (In press).
46. Jun Xie, Shuhuai Huang, Zhengcheng Duan, Yusheng Shi, Shifeng Wen, Correction of the image distortion for laser galvanometric scanning system, Optics and Laser Technology, Volume 37, Issue 4, June 2005, Pages 305-311.
47. Manakov A.; Seidel H-P.; Ihrke I.;, A Mathematical Model and Calibration Procedure for Galvanometric Laser Scanning Systems, Proceedings of VMV, pp.207-214, 2011.
48. Elhawary, H.; Zivanovic, A.; Rea, M.; Davies, B.L.; Besant, C.; Young, I.; Lamperth, M.U.; , "A Modular Approach to MRI-Compatible Robotics," Engineering in Medicine and Biology Magazine, IEEE, vol.27, no.3, pp.35-41, May-June 2008.
49. Li, Yang; Bechhoefer, John; , "Feedforward control of a closed-loop piezoelectric translation stage for atomic force microscope," Review of Scientific Instruments, vol.78, no.1, pp.013702-013702-8, Jan 2007.
50. Chih-Liang Chu, Sheng-Hao Fan, A novel long-travel piezoelectric-driven linear nanopositioning stage, Precision Engineering, Volume 30, Issue 1, January 2006, Pages 85-95.
51. Che Kian Lim; Siyuan He; I-Ming Chen; Song Huat Yeo; , "A piezo-on-slider type linear ultrasonic motor for the application of positioning stages," Advanced Intelligent Mechatronics, 1999. Proceedings. 1999 IEEE/ASME International Conference on , vol., no., pp.103-108, 1999.

52. Awaddy, B.A.; Wu-Chu Shih; Auslander, D.M.; , "Nanometer positioning of a linear motion stage under static loads ," Mechatronics, IEEE/ASME Transactions on , vol.3, no.2, pp.113-119, Jun 1998.
53. L. Juhas, A. Vujanić, N. Adamović, L. Nagy, B. Borovac, A platform for micropositioning based on piezo legs, Mechatronics, Volume 11, Issue 7, October 2001, Pages 869-897.
54. Liu H, Lu B, Ding Y, Tang Y and Li D 2003 A motor-piezo actuator for nanoscale positioning based on dual servo loop and nonlinearity compensation J. Micromech. Microeng. 13 295.
55. Shuichi Dejima, Wei Gao, Hiroki Shimizu, Satoshi Kiyono, Yoshiyuki Tomita, Precision positioning of a five degree-of-freedom planar motion stage, Mechatronics, Volume 15, Issue 8, October 2005, Pages 969-987.
56. Gi Sang Choi; Hie-Sik Kim; Gi Heung Choi; , "A study on position control of piezoelectric actuators," Industrial Electronics, 1997. ISIE '97., Proceedings of the IEEE International Symposium on , vol., no., pp.851-855 vol.3, 7-11 Jul 1997.
57. Wen-Fang Xie; Jun Fu; Han Yao; Su, C.Y., "Observer based control of piezoelectric actuators with classical Duhem modeled hysteresis," American Control Conference, 2009. ACC '09. , vol., no., pp.4221,4226, 10-12 June 2009.
58. Al Janaideh, M.; Ying Feng; Rakheja, S.; Chun-Yi Su; Rabbath, C.-A., "Hysteresis compensation for smart actuators using inverse generalized Prandtl-Ishlinskii model," American Control Conference, 2009. ACC '09. , vol., no., pp.307,312, 10-12 June 2009.

59. Song, G.; Jinqiang Zhao; Xiaoqin Zhou; De Abreu-Garcia, J.A., "Tracking control of a piezoceramic actuator with hysteresis compensation using inverse Preisach model," *Mechatronics, IEEE/ASME Transactions on* , vol.10, no.2, pp.198,209, April 2005.
60. Stepanenko, Y.; Chun-Yi Su; , "Intelligent control of piezoelectric actuators," *Decision and Control, 1998. Proceedings of the 37th IEEE Conference on* , vol.4, no., pp.4234-4239 vol.4, 16-18 Dec 1998.
61. Merry, R.; Kessels, D.; van de Molengraft, R.; Steinbuch, M.; , "Repetitive control applied to a walking piezo actuator," *Control and Automation, 2009. ICCA 2009. IEEE International Conference on* , vol., no., pp.854-859, 9-11 Dec.
62. R.J.E. Merry, D.J. Kessels, W.P.M.H. Heemels, M.J.G. van de Molengraft, M. Steinbuch, Delay-varying repetitive control with application to a walking piezo actuator, *Automatica*, Volume 47, Issue 8, August 2011, Pages 1737-1743.
63. Tan, K.K.; Tong Heng Lee; Zhou, H.X.; , "Micro-positioning of linear-piezoelectric motors based on a learning nonlinear PID controller," *Mechatronics, IEEE/ASME Transactions on* , vol.6, no.4, pp.428-436, Dec 2001.
64. [http : //www.piezomotor.se/products/linear/piezo-legs-linear-6n/](http://www.piezomotor.se/products/linear/piezo-legs-linear-6n/), Piezo Motor, last view in July, 2013.
65. Merry, R.; de Kleijn, N.; van de Molengraft, R.; Steinbuch, M.; , "Control of a high precision stage using a walking piezo actuator," *Control Applications, 2007. CCA 2007. IEEE International Conference on* , vol., no., pp.1285-1290.
66. Merry, R.; de Kleijn, N.; van de Molengraft, M.; Steinbuch, M.; , "Using a

- Walking Piezo Actuator to Drive and Control a High-Precision Stage,” *Mechatronics*, IEEE/ASME Transactions on , vol.14, no.1, pp.21-31, Feb. 2009.
67. Golubovic, E.; Uzunovic, T.; Zhakypov, Z.; Sabanovic, A., ”Adaptive control of piezoelectric walker actuator,” *Mechatronics (ICM)*, 2013 IEEE International Conference on , vol., no., pp.132,137, Feb. 27 2013-March 1 2013.
 68. Skorc, G.; Safaric, R.; Rojko, A.; , ”Polynomial control technique for adaptive positioning within sub-micrometer scale,” *Robotics in Alpe-Adria-Danube Region (RAAD)*, 2010 IEEE 19th International Workshop on , vol., no., pp.131-136, 24-26 June 2010.
 69. Gregor Skorc, Jure Cas, Simon Brezovnik, Riko Safaric, Position Control with Parameter Adaptation for a Nano-Robotic Cell, *Strojniski vestnik - Journal of Mechanical Engineering*, Vol 57, No 4 (2011).
 70. Rong-Jong Wai; Kuo-Ho Su; , ”Supervisory control for linear piezoelectric ceramic motor drive using genetic algorithm,” *Industrial Electronics, IEEE Transactions on* , vol.53, no.2, pp. 657- 673, April 2006.
 71. Merry, R.J.E.; Maassen, M.G.J.M.; Van de Molengraft, M. J G; van de Wouw, N.; Steinbuch, M., ”Modeling and Waveform Optimization of a Nano-motion Piezo Stage,” *Mechatronics, IEEE/ASME Transactions on* , vol.16, no.4, pp.615,626, Aug. 2011.
 72. [http : //www.piezomotor.se/products/drivers/pmcm31/](http://www.piezomotor.se/products/drivers/pmcm31/), PMCM31, last view in July, 2013.
 73. Zhakypov, Zhenishbek and Golubovic, Edin and Kurt, Tark Edip and Şabanoviç, Asif, ”Yürüyen piezoelektrik motorların sürülmesi”, *Otomatik Kontrol Ulusal Toplantı (TOK 2012)*, Niğde: Niğde Üniversitesi, October 2012, 463-468.

74. Edin Golubovic, Zhenishbek Zhakypov, Tarik Uzunovic, Asif Sabanovic, Piezo-electric Motor Driver: Design and Evaluation, (IEEE IES) IECON13 - 39th Annual Conference of the Industrial Electronics Society, Vienna, Austria, (In press).
75. Zhenishbek Zhakypov, Edin Golubovic, Tarik Uzunovic, Asif Sabanovic, Nano-metric Positioning of a Piezo Walker, (IEEE IES) IECON13 - 39th Annual Conference of the Industrial Electronics Society, Vienna, Austria, (In press).
76. F. Szufnarowski and A. Schneider, "Two-dimensional dynamics of a quasi-static legged piezoelectric actuator", Smart Materials and Structures, vol. 21, 2012.